

## Author Queries

- AQ1 Please provide the explanation for the part figure labels (a, b) for the Figure 18.2.
- AQ2 Please provide the explanation for the part figure labels (a, b) for the Figure 18.3.
- AQ3 Please provide the in-text citation for the Figure 18.4.
- AQ4 Please confirm if the edits are okay.
- AQ5 Kindly provide the opening brace for this closing brace.
- AQ6 Kindly provide the opening brace for this closing brace.
- AQ7 Please consider rephrasing for a better clarity.
- AQ8 Please provide the article title for all the journal-type references if possible.

## 18

## AIE-active BODIPY Derivatives

Yali Liu<sup>1</sup>, Yuzhang Huang<sup>1</sup>, Rongrong Hu<sup>1</sup>, and Ben Zhong Tang<sup>2</sup><sup>1</sup>State Key Laboratory of Luminescent Materials and Devices, Guangdong Provincial Key Laboratory of Luminescence from Molecular Aggregates, Center for Aggregation-Induced Emission, South China University of Technology, Guangzhou, China<sup>2</sup>Department of Chemistry, Hong Kong Branch of Chinese National Engineering Research Center for Tissue Restoration and Reconstruction, The Hong Kong University of Science & Technology, Clear Water Bay, Kowloon, Hong Kong, China

## 18.1 Introduction

Organic luminescent materials are a group of important materials for fluorescence-related technologies owing to their advantages such as high sensitivity and selectivity, fast response, easy modification, and low environmental pollution [1, 2]. Of all the organic luminescent dyes, 4,4'-difluoro-o-4-bora-3a,4a-diaza-s-indacene (BODIPY) derivatives are extensively studied classical luminophores with their excellent photophysical properties including stable spectral properties, narrow absorption and emission bands, high-fluorescence quantum yield, high molar extinction coefficient, tunable emission from visible light to near infrared (NIR), and high photo- and chemical stability [3–5], which are widely used in fluorescence sensing and bioimaging [1, 5]. BODIPY compounds were first reported in 1968 by Treibs and Kreuzer [6]. A large number of BODIPY derivatives have been explored since then and applied to solid-state lasers [7, 8], solar cells [9, 10], light harvesting [11, 12], electroluminescent devices [13], fluorescent bioprobes [14, 15], chemosensors [16, 17], etc. The typical synthetic method of BODIPY derivatives is to prepare 8-substituted BODIPY dye (i.e., ones with substituents in the *meso*-position) by condensation of acyl chlorides with pyrroles (Figure 18.1), which generally involve unstable dipyrromethene hydrochloride salt intermediates that are not isolated from the reaction system [5].

The BODIPY molecule without any substitution group is quite emissive with high fluorescence quantum yields in both nonpolar and polar solvents. In THF solution, it emits at 516 nm with a  $\Phi_F$  value of 76.8%. Surprisingly, the molecule is sparingly soluble in water, which emits at 516 nm with a  $\Phi_F$  value of 90.3% [18]. However, due to the self-absorption and strong intermolecular interaction ( $\pi$ - $\pi$  stacking, etc.) caused by their small Stokes shift and planar  $\pi$ -conjugated structures, contrary to their excellent luminescence in solution, most BODIPYs suffer from aggregation-caused emission quenching (ACQ) effect, and show weak fluorescence in the aggregated state, which has greatly limited further application of BODIPYs as a solid-state emitters [19–21].

ACQ effect is actually commonly observed in traditional organic fluorescent dyes with  $\pi$ -conjugated structures, which generally possess excellent luminescence properties in dilute solution, but become weakly or nonemissive in high-concentration solutions or in the aggregated

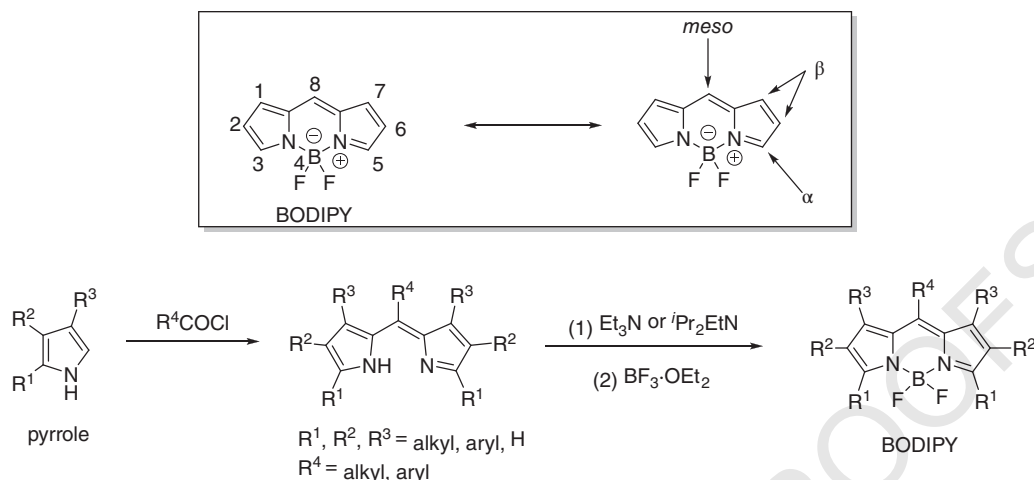


**Figure 18.1** Synthesis and photophysical property of BODIPY.

states. To solve this problem, a new photophysical concept of aggregation-induced emission (AIE) was coined by Tang et al. in 2001, which has rapidly grown into a hot research area and hundreds of AIE luminogens are designed and developed [22–24]. AIE molecules usually possess highly twisted structures and show weak fluorescence in dilute solutions due to nonradiative transition induced by intramolecular motion in their excited state. In the aggregation state, such intramolecular motions are effectively suppressed, resulting in their enhanced emission. Additionally, the highly twisted structure can effectively inhibit the  $\pi$ - $\pi$  interactions between AIE molecules, which is conducive to improving their solid-state luminescence efficiency.

Manipulating BODIPYs with AIE property may be an ideal solution to solve the ACQ problem of BODIPY materials and bring high emission efficiency in the aggregated states. Therefore, the development of BODIPYs with AIE feature has received extensive attention. The first example is to combine twisted intramolecular charge transfer (TICT) and AIE processes in a series of triphenylamine (TPA)-substituted BODIPY derivatives with TPA moiety as the electron donor and the BODIPY moiety as the electron acceptor in 2009 (Figure 18.2) [25]. Take BODIPY derivative **1** for example, it shows both solvent polarity and aggregation-dependent emission behavior. In nonpolar solvents such as hexane, BODIPY compound **1** takes a planar conformation and emits intense green light at 532 nm from locally excited (LE) states; when the polarity of the solvent increases, the conformation of the compound **1** is twisted and the luminogen starts to emit from the TICT state, which causes a large red-shift in the emission maximum and dramatically decreased emission efficiency. In THF solution, compound **1** emitted at 688 nm and an addition of “small” amounts of water weakens and red-shifts its emission, whereas in the aqueous mixtures with “large” amounts of water, the emission is intensified and blue-shifted. Aggregates’ formation or AIE effect has greatly promoted the red emission in the presence of large amounts of water, and the luminogens start to aggregate and emit efficiently. The emission of compound **1** can also be enhanced by increasing solvent viscosity or decreasing solution temperature, which indicates that the restriction of the intramolecular rotations in the aggregated states of the luminogens is responsible for their AIE effect.

In this chapter, we summarized the AIE-active BODIPYs reported in the past few years, the structure–property relationship, and the applications of these BODIPYs.

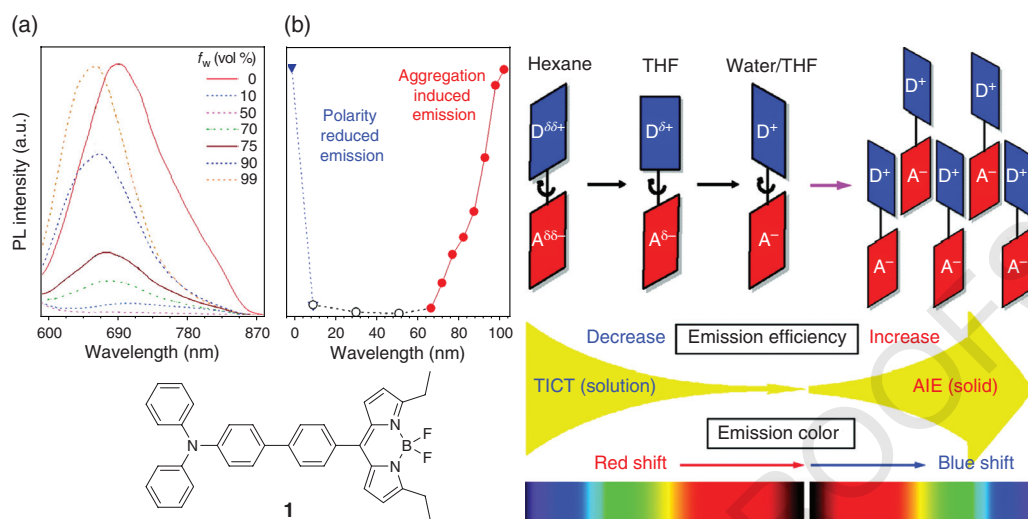


**Figure 18.2** Chemical structure, property of **1** and mechanism for TICT and AIE Processes in BODIPY luminogens. Source: Reproduced with permission from Ref. [25]. Copyright 2009 American Chemical Society.

AQ1

## 18.2 Structures of BODIPY Derivatives

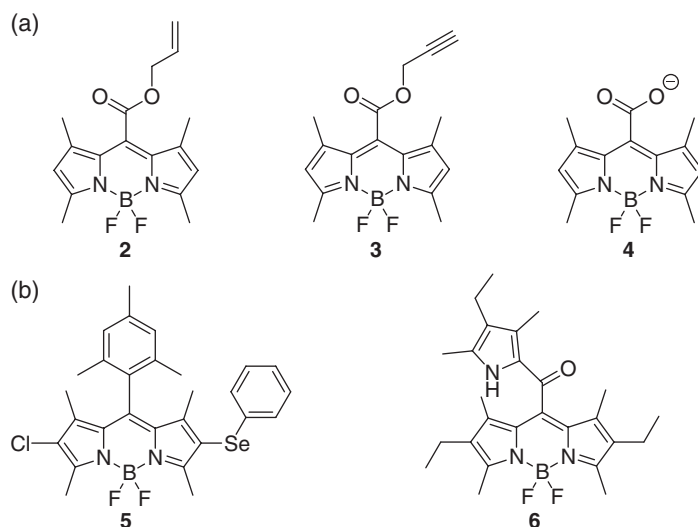
With the great effort that has been made by the chemists and material scientists, a large variety of BODIPY compounds with AIE feature were developed, which have been discussed in eight different categories including BODIPY derivatives without any other chromophore, TPE-containing BODIPYs, TPA-containing BODIPYs, Benzodithiophene-containing BODIPYs, Chiral BODIPYs, Metal-containing BODIPYs, BODIPY-containing polymers, and other BODIPY derivatives.

### 18.2.1 BODIPY Derivatives Without Other Chromophore

Despite that the BODIPY core structure is a coplanar structure and is well known for its ACQ property [26–29], there are a few BODIPY derivatives without any other chromophore been found to possess AIE property (Figure 18.3a). For example, a group of simple BODIPY derivatives **2–4** with carboxylate group substituted on the *meso*-position is reported to show AIE effect [30]. The DMSO solution of compound **2** with an allyl carboxylate group located on the 8-position of tetramethyl group-substituted BODIPY possesses an absorption maximum at 513 nm, while its emission peak is located at 530 nm with its fluorescence quantum yield ( $\Phi_F$ ) lower than 1%. When water is added to the THF solution, the emission intensity of **2** remains almost the same until the water volume fraction ( $f_w$ ) reached 70 vol%. When  $f_w$  continuously increases to 99 vol%, the fluorescence intensity at 591 nm increases dramatically and reaches to maximum with about 100 times increment compared with the THF solution, suggesting the AIE characteristic of compound **2**. Moreover, there is a newly emerged red-shifted absorption band at 589 nm in aqueous mixture of **2**, indicating the formation of *J*-aggregate formation of **2**. Similarly, compound **3** possesses AIE characteristics, and both **2** and **3** display fluorescence response toward  $\text{Pd}^{2+}$  in aqueous buffer, generating compound **4** with strong green emission during the fluorescence detection of  $\text{Pd}^{2+}$ .

A few BODIPY derivatives with only single phenyl ring attached on the core structures have also been found to be AIE-active. For example, a *meso*-mesitylene-BODIPY compound **5** with a





AQ2 **Figure 18.3** Chemical structures of BODIPY derivatives 2–6 without other chromophore.

chloro- and a phenyl selenide-group embedded at the 2,6-position, respectively, of BODIPY core, shows AIE property (Figure 18.3b) [31]. In THF solution, compound **5** emits faintly and shows almost invariable emission intensity when 0–70 vol% water is added into its THF solution. However, when the water fraction increases from 80 to 90 vol%, **5** shows a surge of emission intensity and reaches to maximum at 526 nm when  $f_w = 90\%$ . The emission intensity in 90 vol% aqueous mixture is about 6 times of that in pure THF solution, indicating the AIE characteristic of **5**. Moreover, in a mixed solution of EtOH and 10 mM phosphate-buffered saline (v: v, 1: 2), compound **5** possesses a maximum absorption at 523 nm and a fluorescence quantum yield of 0.16%. After 4.0 equivalent of NaOCl is added to the solution to oxidize the phenylselenium group from selenide to selenoxide structure, the maximum absorption of **5** shifted to 512 nm, the emission maximum slightly changed to 526 nm, and the emission efficiency raised up to 45%, which could be utilized as a fluorescent sensor for hypochlorous acid detection.

In another example, a *meso*-2-ketopyrrolyl-derived BODIPY **6** was synthesized via simple condensation reactions between oxalyl chloride and substituted pyrroles [32]. In  $\text{CH}_2\text{Cl}_2$  solution, the maximum absorption of **6** is located at 534 nm, and the emission maximum of **6** is located at 560 nm with the  $\Phi_F$  value of 21%. When water fraction in acetonitrile/water mixed solution increased to 90 vol%, the emission intensity is increased about 2 times than that in pure acetonitrile, accompanying with a red-shift of the emission maximum to 591 nm. Furthermore, the highly viscose glycerol solution of **6** possesses a high  $\Phi_F$  value of 43%, suggesting the viscosity-sensitive characteristics of **6** which may find perspective application as a viscosity indicator for monitoring living cell activity.

### 18.2.2 TPE-containing BODIPYs

To design AIE-active BODIPYs, one simple approach is to introduce typical AIE functional moieties into the structure [33]. Tetraphenylethene (TPE) is a well-known AIEgen, which could be attached on different positions of BODIPY core through chemical modification, resulting a group of AIE-active TPE-containing BODIPYs [33–36]. For example, compound **7** with a TPE moiety directly attached on the *meso*-position of BODIPY core possesses a LE emission peak at 524 nm

and a TICT emission peak at 630 nm in THF solution. The addition of small amount of water into the THF solution leads to emission quenching, however, when 90 vol% water is added, molecule **7** aggregates and the emission intensity of TICT peak is doubled while the LE emission totally disappears. Moreover, compound **7** possesses a bright-red emission at about 600 nm in the solid state with a large Stokes shift over 100 nm. Multiple TPE units could be attached on the BODIPY core to afford AIE compounds. For example, compound **8** with three TPE moieties directly attached on the BODIPY core at 2,6,8-positions possesses strong emission in both solution and solid states [34]. In THF solution, the emission maximum,  $\Phi_F$  and lifetime values of **8** are 560 nm, 59%, and 4.83 ns, respectively. When less than 60 vol% water is added into the THF solution of **8**, the emission intensity decreases with the  $\Phi_F$  value of 15%; when more water is added, the emission intensity is gradually increased and reaches maximum in 80 vol% aqueous mixture with the  $\Phi_F$  and lifetime value of 60% and 5.18 ns, owing to the formation of amorphous aggregates. Other functional groups besides TPE can be designed in BODIPYs to endow unique functionality to the AIE compound. For example, BODIPY derivative **9** bearing TPE group and a chloro atom at the 3-position is designed to be a fluorescence probe for  $H_2S$ . It absorbs at 550 nm in tris/ $CH_3CN$  buffer solution and possesses dual emission at 438 and 598 nm. After being activated by  $H_2S$ , the probe starts to emit fluorescence at 920 nm with the fluorescence tail that extends to 1300 nm, indicating its potential application as fluorescent probe for identification of colorectal tumors and second near-infrared (NIR-II) imaging. However, the introduction of TPE moieties into BODIPY structure could not guarantee the AIE feature of the resultant compounds. For instance, compound **10** with two directly connected BODIPY core and a TPE moiety attached at each end at the 2-position of BODIPY possesses absorption maximum at 557 nm and emission maximum at 593 nm in THF solution, which are shifted to 566 and 628 nm in the solid state, respectively [35]. The fluorescence quantum yield of **10** in THF solution (53%) and solid state (4%), however, indicate that it is not AIE active. Hence, the AIE property of these TPE-containing BODIPYs is highly dependent on the substitution groups and the structure of linkages, which will be discussed in detail below.

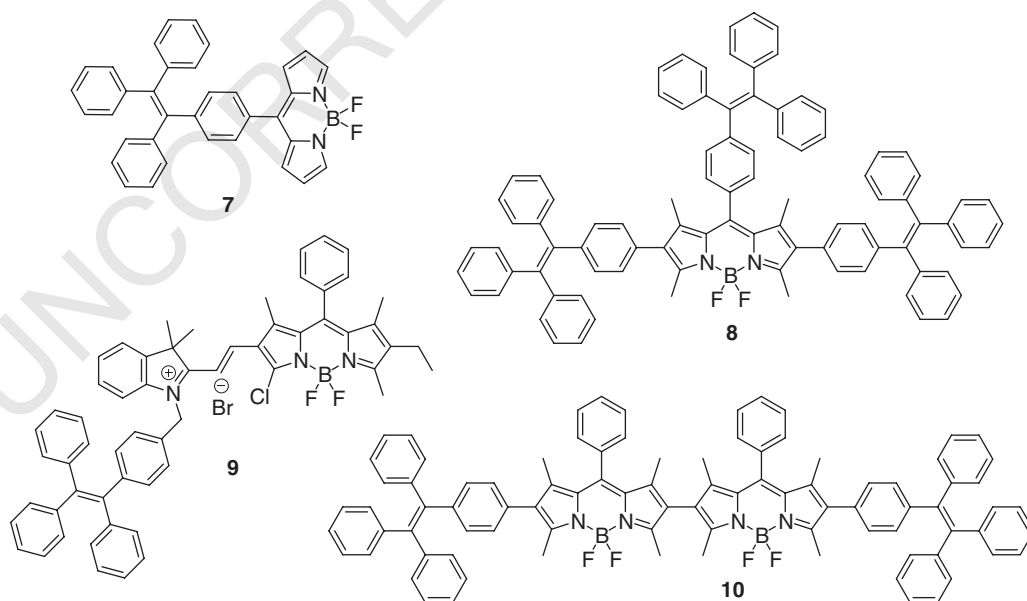


**Figure 18.4** Chemical structures of TPE-containing BODIPYs **7–10**.

AQ3

### 18.2.3 TPA-containing BODIPYs

As another typical AIEgen with strong electron-donating property, triphenylamine (TPA) unit is also frequently introduced into BODIPY derivatives to bring AIE property to the compounds (Figure 18.5) [37, 38]. In these compounds, because of the existence of strong electron donor and acceptor, the emission wavelengths were generally red-shifted compared with other BODIPYs, and these BODIPYs are commonly developed as fluorescence bioprobes for the detection of a series of bioanalytes. For example, a BODIPY derivative **11** with TPA moiety substituted on the *meso*-position of the BODIPY core is designed as a fluorescent sensor for picric acid detection [37]. In THF solution, the absorption maximum and emission maximum of **11** are located at 500 and 649 nm, respectively, which are significantly red-shifted compared with the above-mentioned TPE-containing BODIPYs. **11** is almost nonemissive in pure THF with the fluorescence quantum yield of 0.18%. In THF/water mixtures with the  $f_w$  increases from 0 to 80 vol%, the emission maximum does not show significant shift, while the emission intensity is greatly enhanced by about 350-fold. A similar BODIPY derivative **12** is reported with the fluorescence response toward biothiols to serve as a biocompatible fluorescence probe [38]. A bromo group and a cyano group are attached on the phenyl rings of TPA moiety of **12**, and a 4-aminophenylthio group is attached on the  $\alpha$ -position of BODIPY core. Compound **12** is found to be nearly nonemissive. Upon the addition of cysteine, the DMSO solution of **12** absorbs at 480 nm and emits at 549 nm with the  $\Phi_F$  value of 11%, which can serve as a fluorescence turn-on probe using cyano group as the recognition site to form five- or six-membered rings with Cys or Hcy, respectively, leaving the *p*-aminophenylthio moiety unreacted to form emissive products such as compound **13**.

Another design is realized in a red-emissive fluorophore **14** as scaffold for bovine serum albumin (BSA) sensor, where TPA is directly linked on the *meso*-position of 1,3,5,7-tetramethyl substituted BODIPY core, and two benzoic acid-containing vinyl groups are attached on the other two phenyl rings of the TPA group [39]. There are two emission bands of the THF solution of **14** at 525 and 652 nm, and emission is observed at 636 nm in the THF/water mixture of **14** with 90 vol% water content. The fluorescence quantum yield of **14** has increased from 5% in THF solution to 10% in

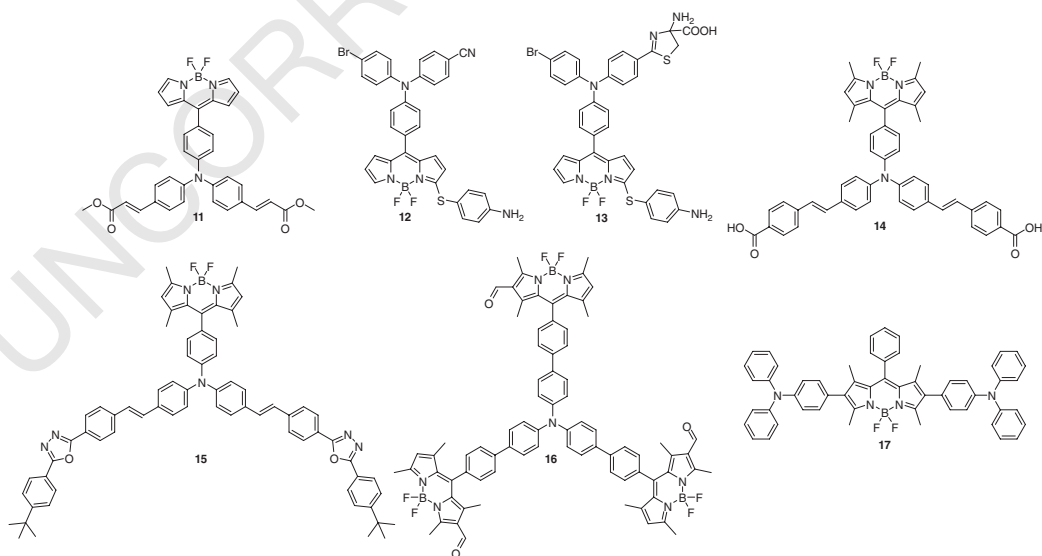


**Figure 18.5** Chemical structures of TPA-containing BODIPYs **11–17**.

the 90 vol% aqueous mixtures, revealing its AIE property. Meanwhile, the emission intensity at 525 nm decreases, due to the increased polarity of the solvent system. Based on this structure, a new oxadiazole building block is modified on the stilbene moiety in TPA-BODIPY derivative **15** through a palladium-catalyzed Heck reaction [40]. The THF solution of **15** is absorbed at 500 nm, while it exhibits a red emission peak at 647 nm as the main peak and a weak green emission peak at 513 nm, and the fluorescence  $\Phi_F$  at 647 nm is 11%. When small amount of water is added into the THF solution, the polarity increases and both emission peaks are quenched. In 90 vol% aqueous mixtures, the emission maximum is shifted to 628 nm and the emission intensity approaches the highest level. The solid powder of **15** shows strong red emission at 614 nm.

A  $C_3$ -symmetric, TPA-decorated BODIPY compound **16** is also synthesized with three 2-formyl-1,3,5,7-tetramethyl BODIPY units linked at each phenyl ring of the TPA core through a phenyl-ring spacer to furnish an electron donor-acceptor structure [41]. Compound **16** absorbs at 495 nm and emits at 538 nm in THF solution, and the solution fluorescence  $\Phi_F$  value is 21%. When more than 20 vol% of glycerol is added into the DMSO solution of **16**, the emission intensity is enhanced, which becomes  $\sim 2.3$ -fold higher in the DMSO/glycerol mixture with 90 vol% glycerol than that in DMSO solution. It is also demonstrated that **16** shows fluorescence response toward  $F^-$  and  $CN^-$  through the preferential binding of  $F^-$  and  $CN^-$  at the boron center of BODIPY core to cause decomposition, which could potentially be developed as a fluorescent sensor for such anions.

Except for *meso*-position linkage, the TPA moieties could also be attached to other positions on BODIPY core structure. For example, compound **17** with two electron-donating TPA groups attached on the 2- and 6-positions of the electron withdrawing BODIPY core and a phenyl ring substituted on the 8-position of BODIPY are synthesized through Suzuki cross-coupling [42]. In acetonitrile solution of **17**, faint emission is observed at 668 nm with a shoulder peak at 412 nm and the  $\Phi_F$  value of 0.3%. When water is added into the acetonitrile solution, the emission intensity of **17** is dependent on the water fraction: when small amount of water below 60 vol% is added, the fluorescence intensity increases upon the addition of water and reaches maximum in 60 vol% aqueous mixture; when  $f_w$  is further increased from 60 to 90 vol%, the emission intensity is gradually decreased due to the simultaneous formation of crystalline particles and amorphous particles. Furthermore, the low cytotoxicity of **17** enables its application in HeLa cells as a biocompatible fluorescent probe.

AQ4

#### 18.2.4 Benzodithiophene-containing BODIPYs

Benzodithiophene is a useful class of synthons for the design of D-A type systems, which is a suitable ambient stable donor owing to its planar structure, deep lying HOMO levels, and facilely tuned optical properties through structural modification [43, 44]. The combination of benzodithiophene and BODIPY could afford strong electron donor-acceptor structures with electron-rich benzodithiophene served as electron donor and electron-poor BODIPY unit served as electron acceptor, which could bring interesting photophysical property, especially solvent polarity-sensitive luminescence. A series of regioisomeric benzodithiophene-containing BODIPYs **18–23** were reported by Sengupta et al., which possessed twisted electron donor-acceptor structure and TICT characteristics (Figure 18.6) [43–45]. For compounds with one BODIPY moiety and one benzodithiophene moiety from compound **18** with these two groups substituted on the *meso*-position of a benzene ring to compound **19** with these two groups substituted on the *para*-position of a benzene ring, a slightly red-shifted emission at 647 nm is observed for compound **19** compared with that of **18** at 638 nm in chloroform solutions. When the solvent polarity decreases from THF

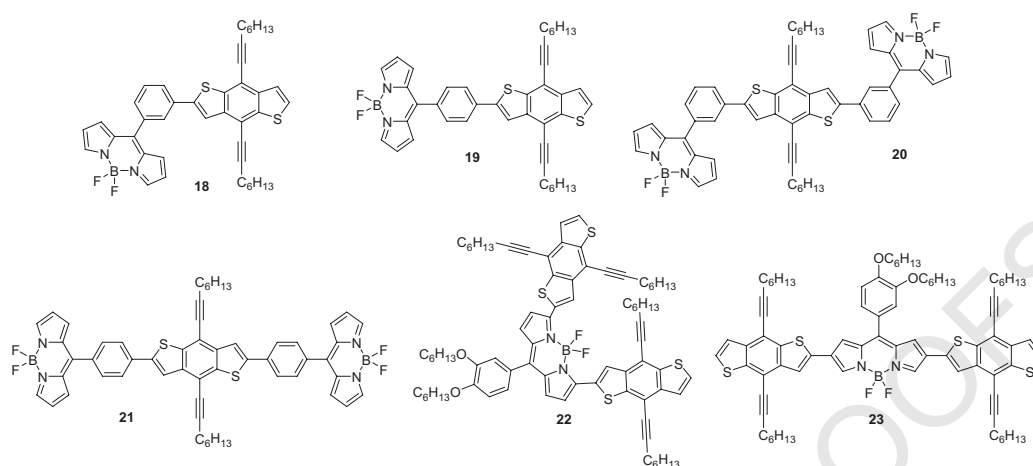


**Figure 18.6** Chemical structures of benzodithiophene-containing BODIPYs **18–23**.

to 99 : 1 of hexane/THF, compound **19** exhibits an obvious hypsochromic shift to about 523 nm, indicating the locally excited emission in nonpolar solvents, and TICT emission in polar solvents [45]. For compounds consisting of two BODIPY units and one benzodithiophene unit, the *para*-substituted isomer **21** has a similar bathochromic shift at 698 nm in the emission maximum of THF solution compared with that of the *meso*-substituted isomer **20** at 662 nm. However, the solvent-dependent emission behavior is quite different. In THF solution, **21** possesses large twisted angles between BODIPY and phenyl spacer, as well as between phenyl spacer and benzodithiophene unit, which possesses a large pseudo-Stokes shift of about 194 nm and a positive fluorescence solvatochromism, indicating the formation of TICT state; while **20** does not display any TICT emission, probably because there is weak electronic coupling between the donor and acceptor through the *m*-phenylene connection. Compounds **18–20** show a typical AIE effect. In general, a decline in fluorescence intensity first occurs when small amount of water is added into the THF solution because the increasing solvent polarity may promote TICT process and nonradiative deactivation; large volume of water then causes aggregates formation and emission enhancement. For compounds with one BODIPY core and two benzodithiophene units linked directly on the BODIPY core from 3,5-position (**22**) and 2,6-positions (**23**) without any spacer between the electron donor and acceptor, they both possess high structural rigidity and involve photo-induced electron transfer process with fast decay and short lifetime. The efficient electron transfer in compound **23** quenches its fluorescence with a nonradiation deactivation process. Compound **23** (lifetime ~0.46 ns) shows a faster decay compared to that of **22** (~3.16 ns), suggesting that **23** possesses more efficient photo-induced electron transfer than **22**.

### 18.2.5 Chiral BODIPYs

Chiral luminophores are a group a fascinating material, owing to their potential applications in circularly polarized luminescence (CPL), which has attracted growing attention in the development of new optical devices, advanced display technologies, and enantioselective sensors [46, 47]. Despite that many different chiral luminescent materials have been developed for their potential application in CPL, materials with red-emissive CPL signals in the aggregated states have been rarely reported. One strategy to realize red-emissive solid-state CPL signal is to integrate AIE

functional group and chiral groups into BODIPY compounds. For example, with electron donor and acceptor structure, BODIPY derivatives could be red emissive. The introduction of typical AIEgen, TPE, would bring strong aggregated state emission to BODIPY, and an optically active 1,10-binaphthol (BINOL) can endow the compound with a chiral configuration, hence lead to CD and CPL signal.

Based on this strategy, Zhu et al. reported two chiral enantiomers (*R*)-**24** and (*S*)-**25** with two TPE groups linked at the 2,6-positions of BODIPY core through a C≡C bond spacer and the *R*-BINOL and *S*-BINOL moieties attached on the boron atom through boro-ester bonds in (*R*)-**24** and (*S*)-**25**, respectively (Figure 18.7) [48]. Their maximum absorbance wavelength in dichloromethane solution is located at 580 nm, and they exhibit emission at 618 nm in dichloromethane, which are typical red-emissive luminophores. Moreover, these molecules both possess typical AIE properties, which show low fluorescence quantum yield of 1.4% in dichloromethane solution and up to 58.2% high  $\Phi_F$  value in the dichloromethane/hexane mixed solution with 90 vol% hexane. Besides, their CD peaks appear at 580 nm, suggesting the successful transfer of chirality from BINOL to BODIPY moiety. Most importantly, the mirror-image red-color CPL signals from these compounds were induced by intramolecular energy transfer and these two compounds exhibit CPL signals at 630 nm with the optical anisotropy factor ( $g_{lum}$ ) values of about 0.002, which are comparable to the reported organic CPL materials ( $10^{-5}$ - $10^{-2}$ ), suggesting their potential application as CPL materials [49].

Similarly, Tang et al. reported a pair of chiral enantiomers (*R*)-**26** and (*S*)-**27** with the TPE moiety directly attached on the *meso*-position of BODIPY core and the *R*-BINOL and *S*-BINOL attached on the boron atom through boro-ester bonds in (*R*)-**26** and (*S*)-**27**, respectively [50]. In both compounds, TPE moiety acts as a dark energy donor and BODIPY as an energy acceptor. Both compounds emit strong green fluorescence at 517 nm in THF with a fluorescence quantum yield of 89%. The emission is gradually enhanced with the addition of hexane into THF, suggesting typical AIE characteristic. Moreover, two CD absorbance bands at 340 and 507 nm are observed for (*R*)-**26**

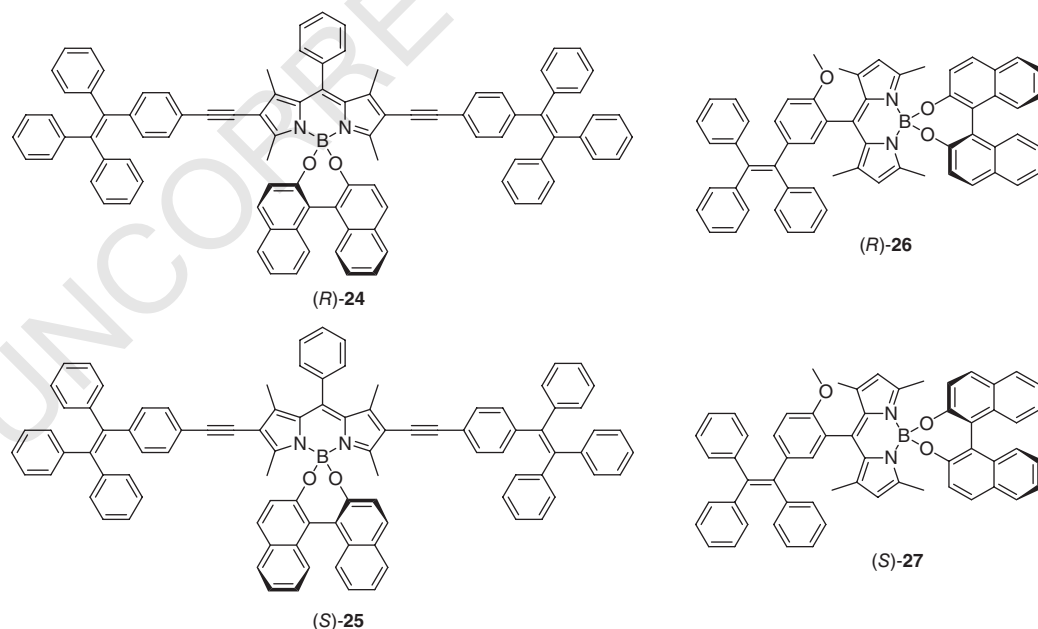


**Figure 18.7** Chemical structures of chiral BODIPYs **24–27**.



AQ5,6

and (*S*)-**27**, corresponded to the TPE and BODIPY moieties, respectively, indicating that the chirality of TPE and BODIPY groups are induced by BINOL. As expected, a mirror image of CPL signals with  $g_{\text{lum}}$  values of -0.0027 (*R*)-**26** and 0.0041 (*S*)-**27** are observed from their THF solutions. No obvious change happens when water is added. They exhibited high fluorescence quantum yield and large pseudo-Stokes shift of 167 nm via dark through-bond energy transfer, which overcomes the background interference between excitation and emission.

### 18.2.6 Metal-containing BODIPYs

Transition metal could also be introduced into BODIPY derivatives to afford a series of multifunctional optical materials with variable photophysical properties, considering that metal-based complexes are widely used in host-guest chemistry, sensing, and anticancer treatment, etc. [51]. Of all the metal complexes, Pt(II) diimine acetylide complexes are known to possess unique photophysical characteristics including long triplet excited-state lifetime and high triplet quantum efficiency, due to their heavy-atom-induced, strong-spin orbital coupling. Attracted by these advantages of Pt(II) complexes, Pt(II)-BODIPY complexes **28** and **29** with BODIPY-containing acetylide ligand and carbazole or fluorene-containing bipyridine coordinated on the Pt(II) ion are designed and synthesized (Figure 18.8) [52]. In acetonitrile solutions of **28** and **29**, only weak emission at about 510 nm is observed. When poor solvent water is gradually added, the emission intensity is significantly increased, which reaches maximum in 50 vol% aqueous mixture. Further addition of water has leads to decrease of emission intensity. The triplet excited-state lifetimes of complexes **28** and **29** exhibit similar trend, which are gradually increased with the increment of water and reach 2.5  $\mu\text{s}$  (**28**) and 1.4  $\mu\text{s}$  (**29**), respectively, in 60 vol% aqueous mixture. It is noted that their decline of

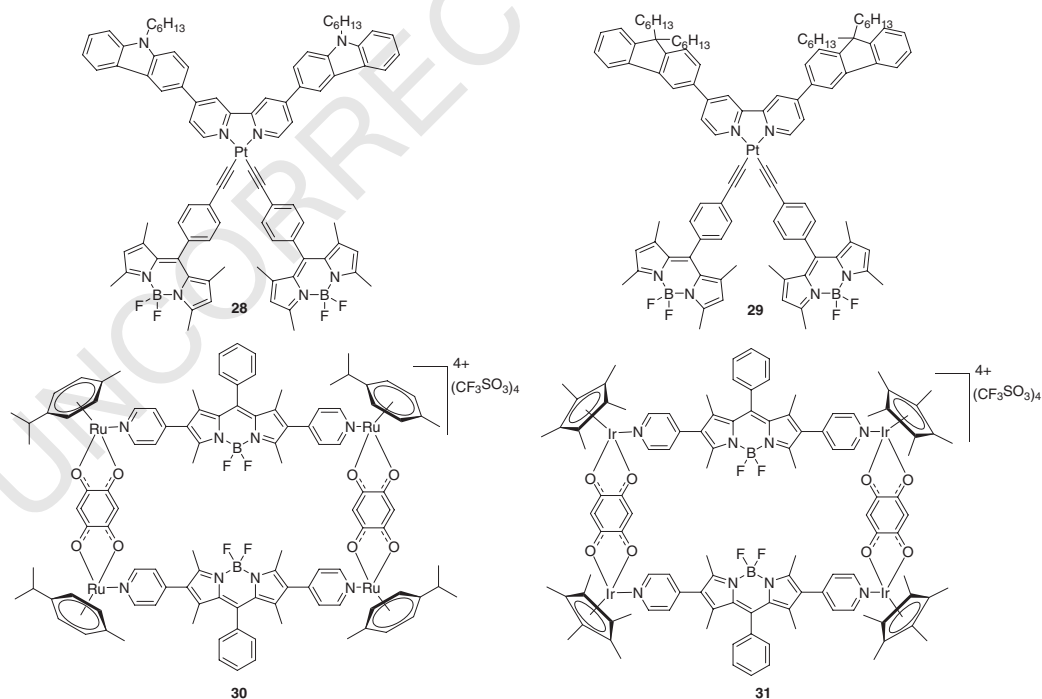


**Figure 18.8** Chemical structures of metal-containing BODIPYs **28–31**.



output energy density occurs with the increment of the incident energy density, suggesting the occurrence of reverse saturable absorption in these Pt(II)–BODIPY complexes.

Supramolecular complexes of Ru(II) and Ir(III) are also well-studied as potential anticancer agents. Hence, it is beneficial to construct BODIPY-containing Ru(II) and Ir(III) complexes to endow unique fluorescence behavior to the supramolecules with the coexistence of monomeric and aggregated species. A group of Ru(II) and Ir(III) complexes are reported with BODIPY-containing pyridine, quinone, and benzene ring/cyclopentadiene ions coordinated on the metal ions to form multinuclear metal complexes [53]. The complexes **30** and **31** both exhibit strong absorption band at about 520 nm in CH<sub>3</sub>CN solution originated from the  $n-\pi^*$  transition of BODIPY moiety. Besides, the complexes inherit an emission peak at ~537 nm from BODIPY moiety in CH<sub>3</sub>CN solution and show a typical AIE feature when the complexes are aggregated inside the cell. The anticancer feature from Ru(II) and Ir(III) further endows these complexes with highly selective anticancer activity and strong interaction with DNA and RNA, demonstrating an effective strategy for the construction of fluorescent anticancer medicine.

### 18.2.7 BODIPY-containing Polymers

AIE polymers with improved processability can also be prepared from BODIPY-containing building blocks through a series of polymerization methods including free-radical polymerization, Sonogashira polycoupling, and Suzuki-Miyaura polycoupling. For example, polymer **32** is a random copolymer synthesized from the radical copolymerization of BODIPY monomer (BO) and styrene (St) (Figure 18.9) [54]. Multicolor and efficient emission in the aggregated state can be realized by tuning the length of polystyrene spacer. By changing the content of BO from 100 to 0.042 mol%, the emission color of **32** can vary from red to green in the wavelength range of 549–757 nm, and the fluorescence quantum yield also increases accordingly from 5 to 88%, owing

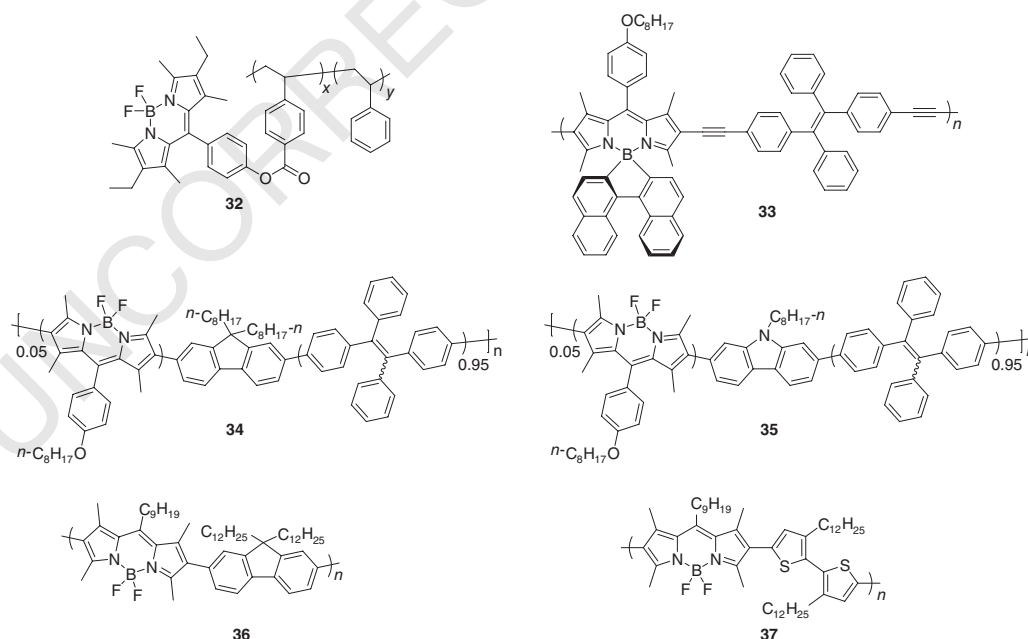


**Figure 18.9** Chemical structures of BODIPY-containing polymers **32**–**37**.

to the elongated distance among the BO fluorophores. When the content of BO is 0.042 mol%, the maximum emission is located at 538 nm in THF solution with the  $\Phi_F$  value of 65%. In bulk film state, **32** shows a maximum emission peak at 545 nm with the  $\Phi_F$  value of 75%.

Recently, an AIE-active conjugated polymer **33** with red emission at 610 nm in dichloromethane solution is prepared through palladium-catalyzed Sonogashira coupling reaction from a chiral BODIPY monomer and TPE-containing diyne monomers, whose nanoparticles are found to possess excellent photostability, remarkable biocompatibility, and so on [55]. In these conjugated polymers, long, flexible aliphatic alkyl chains are frequently introduced on BODIPY moieties to increase the solubility of the resultant polymers. When hexane is added to the dichloromethane solution, the emission intensity of **33** gradually increases and reaches sixfold higher in 90 vol% hexane mixture than that in pure dichloromethane solution. Furthermore, another group of conjugated polymers **34–37** are prepared through Suzuki coupling polymerization of BODIPY, TPE, fluorene, carbazole, or bithiophene building blocks to afford AIE polymers with electron donor–acceptor structures [56, 57]. Take polymer **34** for example, with the water fraction in THF/water mixture increasing from 0 to 40%, **34** exhibits an obvious fluorene emission signal, which decreases and completely disappears when  $f_w > 60$  vol%; On the other hand, the emission peak at 575 nm gradually increases upon the addition of water and reach a  $\Phi_F$  value of 16% with the  $f_w$  of 80 vol%. Compared with polymer **34** with BODIPY, TPE, and fluorene moieties, when the fluorene group is replaced by a strong electron-donating carbazole moiety in polymer **35**, a relatively weak emission and obvious red-shift is observed in their emission from 578 to 598 nm. This simple tuning of polymer composition is hence demonstrated to be a convenient strategy to develop AIE-active low-potential electrochemiluminescence (ECL) materials with low potential and high ECL emission.

### 18.2.8 Other BODIPY Derivatives

There are also several other BODIPY derivatives incorporated with unique functional groups that are reported to possess AIE feature with their structures shown in **Figure 18.10** [58–63]. For example, a piperazine-bridged naphthalimide BODIPY compound **38** is reported which absorbs at 498 nm and emits at 626 nm in THF solution [58]. The electron donor/acceptor system of compound **38** could induce TICT process in polar environment and hence show solvatochromism effect. The strongest emission of **38** was observed in nonpolar solvent hexane at 521 nm, which is gradually red-shifted and quenched upon increasing of solvent polarity and emits faintly at 640 nm in polar solvent methanol. In THF/water mixtures, the emission intensity does not affect much when 0–70 vol% water is added into the THF solution, while the emission intensity is enhanced significantly with a red-shift in the emission maxima from 70 to 99 vol% aqueous mixtures, and the  $\Phi_F$  value of 99 vol% aqueous suspension (15.5%) is much higher than that of the THF solution (8%), accompanying with a 113-nm red-shift. The solid powder of **38** emits at 630 nm with the  $\Phi_F$  value of 13.39%, which is enhanced than its solution, demonstrating its AIE property. In another work, a unique 2,2'-biindenyl moiety is introduced into BODIPY **39**, whose fluorescence is sensitive to solvent and molecular alignment in crystal states [59]. In nonpolar solvent toluene, a single sharp emission peak is observed at 529 nm, while in polar solvent THF, besides the emission peak around 524 nm, a new emission peak emerges at 665 nm. When small amount of water is added into THF solution, the red emission at 665 nm is quenched, and the emission band at 543 nm gradually increases and reaches maximum in 70 vol% aqueous mixture. Compound **39** can form polymorphs from different solvents: orange-emissive crystals can be obtained from chloroform and red-emissive crystals can be afforded in dichloromethane, demonstrating tunable solid-state emission color from 582 to 661 nm. In addition, the solid-state emission color of these compounds could be tuned

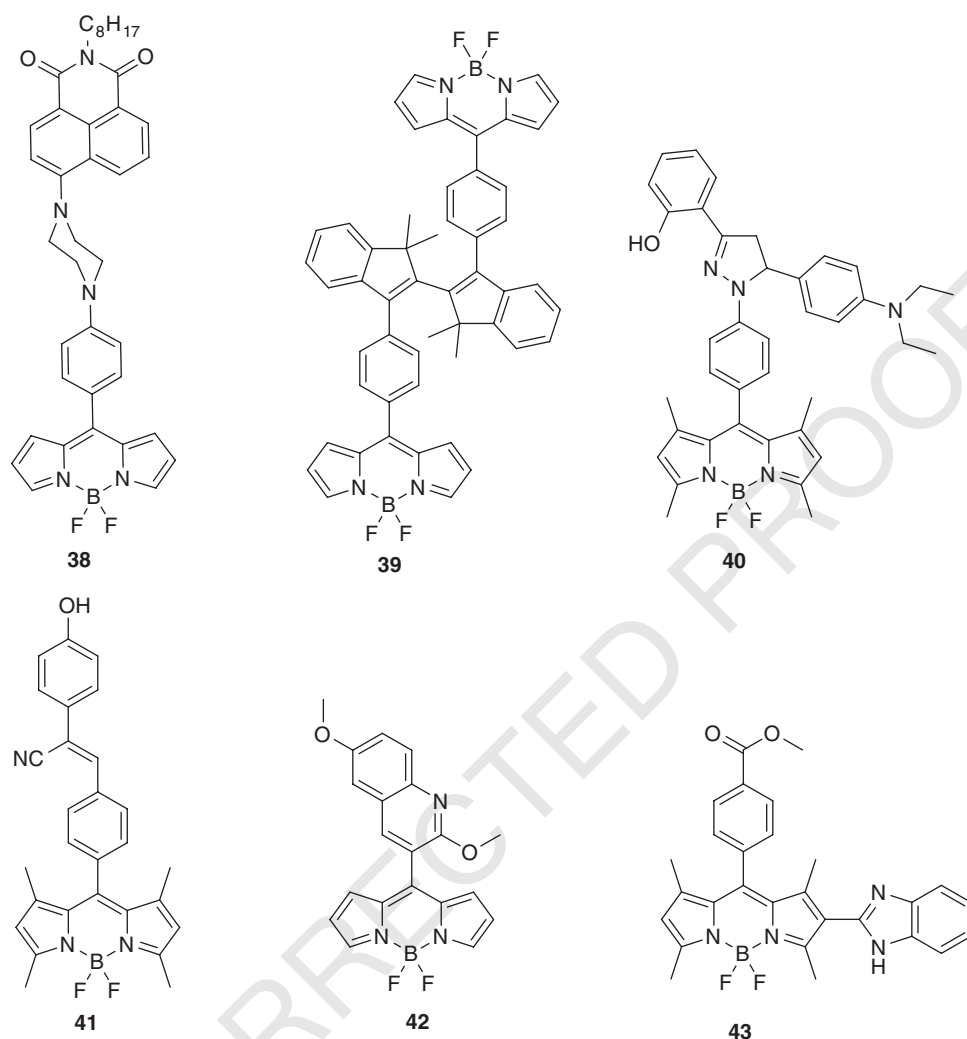


**Figure 18.10** Chemical structures of other BODIPY derivatives **38–43**.

from blue to red (417–661 nm) by the variation of substituents on the 2,2'-biindenyl units. Moreover, compound **40** with a pyrazoline unit linked at 8-position of BODIPY is built from a condensation reaction, which absorbs at 500 nm and emits at 638 nm in THF solution [60]. When small amount of water (10 vol%) is added to the THF solution of **40**, the emission is quenched and red-shifted due to the increased polarity induced TICT process; when more than 70 vol% water is added, the emission of **40** recovers, owing to the AIE effect of the compound and the strongest emission is observed in 99 vol% aqueous mixture. Compound **40** can also self-assemble to form nanoparticles with excellent photophysical properties, prominent water-dispersibility, and stability, as well as distinguished biocompatibility.

An AIE-active cyano-diphenylethylene-conjugated BODIPY compound **41** is prepared as a pH probe from the condensation reaction of 4-hydroxybenzene acetonitrile and 4-(diethoxymethyl) benzaldehyde, which absorbs at 505 nm and emits at about 530 nm in THF solution [61]. Upon addition of water into the THF solution of **41**, the emission is quenched and the fluorescence

intensity is then gradually increased after large amount of water is added and eventually reaches maximum at 80 vol% aqueous mixture, accompanying with a 138-nm red-shift. The phenol moiety of **41** can be easily deprotonated to phenolate anion under basic condition, and the electron-rich substituents usually quench the fluorescence of BODIPY, and large pH values could hence decrease the fluorescence intensity. With the pH-dependent fluorescence response, a pH sensor based on compound **41** is designed as  $\text{CO}_3^{2-}$ -detector among 13 kinds of common anions both in solution and by tested strips. On the other hand, compound **42** with two methoxyl group-substituted quinoline-conjugated BODIPY structure is found to emit at about 434 and 530 nm in methanol solution [62]. The addition of water into methanol solution of **42** gradually quenches the emission, until 80 vol% water is added to induce two new emission bands peaked at 567 and 614 nm. Similarly, the fluorescence lifetime of **42** is also enhanced from 1.10 ns in methanol to 3.89 ns in water/methanol mixture with 90 vol% water content, indicating the formation of nanoaggregates of **42**. The nanofibers of **42** can be further encapsulated with BSA matrix to afford nanoparticles for in vivo cell imaging. In another work, a pH-sensitive proton acceptor benzimidazole unit is substituted on 2-position of BODIPY to afford compound **43** [63]. In neutral PBS buffer, dual emissions are observed for **43**: the emission peak at 510 nm is attributed to the intrinsic emission from BODIPY core, together with another red peak at about 595 nm. When the pH of solvent is decreased from 7.2 to 6.5, the emission peak at 625 nm is quenched while that at 488 nm is increased. This could also be observed under UV lamp irradiation by naked eyes, the emission color changes from red to bright green upon acidification from pH value of 6.0–1.0. The solid state of **43** emits at 645 nm. The application of **43** in intracellular pH calibration by ratiometric imaging will be introduced below.

Except for classical BODIPYs, there are different variations on the BODIPY core, which could also afford AIE-active BODIPY analogues. A few examples are shown in **Figure 18.11**. Based on the three fused ring structures from classical BODIPYs, if the carbon atom at the 8-position of the BODIPY core is replaced by a nitrogen atom, AIE-active boron-difluoride complexes could still be designed [64, 65]. For example, compound **44** with a planar aza-boron-diquinomethene

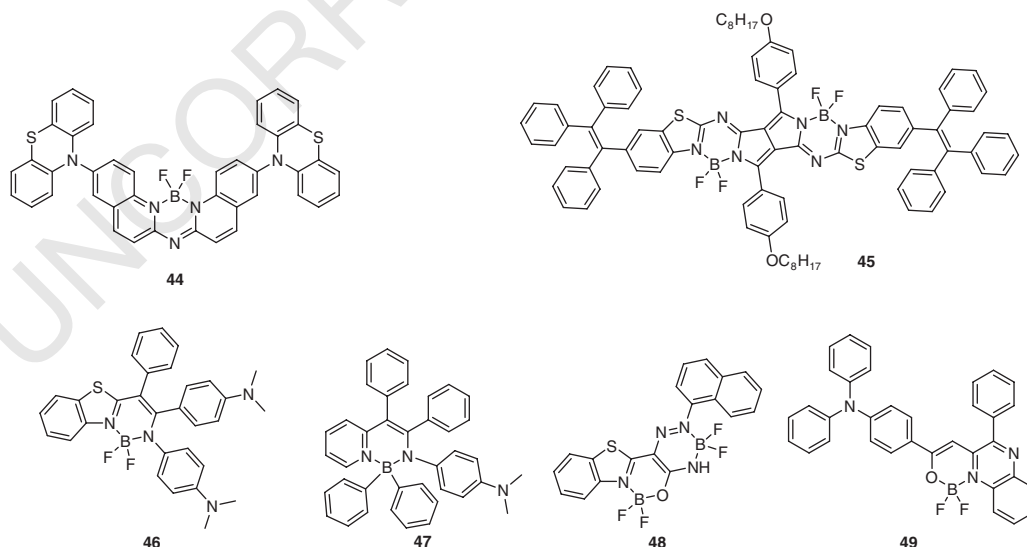


**Figure 18.11** Chemical structures of other BODIPY analogues **44–49**.

core and two phenothiazine chromophores attached is synthesized by a one-step Buchwald–Hartwig coupling reaction, which possesses switchable emission ranging from blue to yellow to red in THF/water mixtures. The THF solution of **44** emits blue light at 480 nm while its solid powder emits yellow light at 540 nm, and its 90 vol% aqueous solution emits at 610 nm with increased emission intensity compared with the solution. The single crystal structure of compound **44** indicates a highly vertical twisted conformation between the phenothiazine rings and the planar aza-boron-diquinomethene core, which adopts a H-type stacking aggregation via intermolecular C–H...F,  $\pi$ – $\pi$ , and C–H... $\pi$  interactions, leading to TICT effect and red-shifted emission. The appearance and emission color of **44** can also be switched via multiple external stimuli such as grinding, vapors of organic solvents, acid, or base. Another red-emissive symmetric triphenylethene-modified pyrrolopyrrole aza-BODIPY molecule **45** with eight fused rings is found to emit faintly in THF solution at 697 nm with the  $\Phi_F$  value of 1.1%, and in CH<sub>2</sub>Cl<sub>2</sub> solution at 699 nm with the  $\Phi_F$  value of 0.4%. However, when 90 vol% hexane is added in the CH<sub>2</sub>Cl<sub>2</sub> solution of **45**, the nanoaggregate absorbs at 690 nm and emits intensely at 710 nm with the  $\Phi_F$  value of 18.8%. The introduction of AIEgen triphenylethylene can break its panel-like structure to inhibit their  $\pi$ – $\pi$  stacking and endow compound **45** aggregation-enhanced emission feature in NIR region.

The pyrrole ring on the BODIPY core could also be replaced by other aromatic rings such as thiophene [66, 67]. For example, a benzothiazole-enamide-based boron difluoride complex **46** is synthesized through the reaction of benzothiazole-enamide-based unsymmetric *N,N*-bidentate ligands with boron trifluoride etherate. Compound **46** emits weakly in THF solution at 448 nm with the fluorescence quantum yield of 2%, and emits intensely in the solid state at 555 nm with a high  $\Phi_F$  of 23%. The emission intensity of 80 vol% aqueous solution of **46** in THF/water mixture is significantly increased with the  $\Phi_F$  value of 20%, which is 10 times higher than that in pure THF solution. In addition, compound **46** is capable of sensing acidic gas by reversible changes of fluorescence, which may potentially serve as acidic vapor sensor. Another pyridyl-enamido-based organoboron complex **47** also shows AIE property, which possesses weak emission at 513 nm in CH<sub>2</sub>Cl<sub>2</sub> solution with the  $\Phi_F$  value less than 1%, and strong emission at 577 nm in the solid state with a high  $\Phi_F$  value of 10%. In THF/water mixtures with gradual addition of water, the emission maxima dramatically shifts from 513 to 583 nm, owing to the AIE enhancement of TICT state. An acidic/basic gas-triggered solid-state emission change is also observed for compound **47**. A filter paper coated with **47** emits orange light under UV irradiation, which changes to green upon exposure to HCl vapors as a result of the protonation of the amino group. The propeller-shaped conformations in compounds **46** and **47** significantly prevents the formation of the undesirable  $\pi$ – $\pi$  stacking between two planar BODIPY cores in solid or aggregated state, leading to typical AIE effect.

When one of the two coordination atoms linked on boron atom in BODIPY core has changed from nitrogen to oxygen atom, the resultant compounds could also be designed to be AIE active [68, 69]. For example, a benzothiazole-hydrazone chelate-based bisboron complex **48** is reported to emit at 560 nm in the solid state. Compounds **46–48** generally show weak emission in solvents with low viscosity because the intramolecular rotation has facilitated nonradiative process which consumes excited-state energy and quenches emission. Their emission can be dramatically enhanced by either increasing the solvent viscosity or molecular aggregation in the solid state. Last but not least, a quinoxaline- $\beta$ -ketoiminate boron-difluoride complex **49** is reported with tunable emission. It emits at 617 nm in CHCl<sub>3</sub> solution with a  $\Phi_F$  value of 10%. While its emission behavior does not change much in the solid state, a reversible on–off solid-state emission switching of **49** can be realized by acid/base vapors fuming processes.

### 18.3 Structural–property Relationship

While there are a great number of AIE-active BODIPY luminophores been reported, their photo-physical properties such as conjugation, steric hindrance, the type, number, and position of substitution groups are highly dependent on their structures, which will be discussed with detailed examples as shown below. Most examples discussed here are based on the largest AIE-active BODIPY family: TPE-containing BODIPY compounds.

#### 18.3.1 Conjugation Effect

First, the conjugation effect on the AIE property is investigated from a series of TPE-containing BODIPYs **50–52** with different linking bridge groups (C–C, C=C, C≡C) prepared from the palladium-catalyzed cross-coupling reactions such as Suzuki coupling, Heck reaction, and Sonogashira reaction, respectively [70]. THF/water mixtures are used to study their aggregation-dependent emission behaviors. Compound **50** with C–C single bond spacer possesses emission peak at 524 nm with a shoulder peak at 650 nm in THF solution, which is decreased upon the addition of water; compound **51** with C=C spacer possesses the best conjugation among all the three compounds, which mainly emits at 640 nm in THF solution and the increased intensity upon the addition of large amount of water; compound **52** with C≡C bonds spacer with the conjugation in between C–C and C=C spacer mainly emits at 529 nm, whose intensity is decreased upon the addition of water, accompanying with a newly emerged strong emission peak at about 600 nm (Figure 18.12). In these emission spectra of THF/water mixtures, the green emission peak around 524 nm is attributed to the emission from LE state of the molecules, while the red emission peak around 640 nm is attributed to the emission from TICT state. Increasing the water content in these aqueous mixture generally increases the TICT emission intensity of **51** and **52**, while it decreases the LE emission intensity of **50** and **52**. Meanwhile, the fluorescence quantum yields ( $\Phi_F$ ) of **50–52** are determined, suggesting that the solid-state fluorescence quantum yields of **51** and **52** are 27 and 7.5%, respectively, which are much higher than the  $\Phi_F$  values of **50–52** in THF solution in the range of 0.1–0.3%. Hence, compound **51** with the best conjugation of all the three molecules possesses an AIE-active TICT emission peak, compound **50** with poor conjugation spacer possesses a LE emission peak which is ACQ, and compound **52** possesses both AIE-active TICT emission and ACQ-active LE emission. The green and red dual emission of **52** enables its application as fluorescent visualizer for intracellular imaging.

#### 18.3.2 Number and Position of Substitutes

The effect of the number of TPE groups and their substituted positions on BODIPY core on the AIE property are also studied from a series of BODIPY–TPE derivatives [71, 72]. For example, one or two TPE groups are attached on the 3,5-positions of BODIPY core through C=C spacer in compounds **53** and **54**; an additional TPE group is directly attached on the *meso*-position of the BODIPY core in **55–57**, and their emission in THF/water mixtures is systematically studied (Figure 18.13) [71]. As can be seen from the fluorescence image, the THF solutions of **53**, **54**, **56**, and **57** all emit red light in the wavelength range of 610–690 nm, which are generally quenched upon addition of water, suggesting that aggregation causes fluorescence quenching in these compounds. However, compound **55** with only one TPE group on the *meso*-position of BODIPY possesses an ACQ green emission at 530 nm and an AIE red emission at 620 nm. When water is gradually added into the THF solution, the fluorescence of **55** changes from green to orange. It can be concluded that TPE substitution





**Figure 18.12** Chemical structures of **50–52**. Photoluminescence spectra of (a) **50**, (b) **51** and (c) **52** in THF/water mixtures with different water fractions ( $f_w$ ). *Source:* Reproduced from Ref. [70]. Copyright 2012 Royal Society of Chemistry.



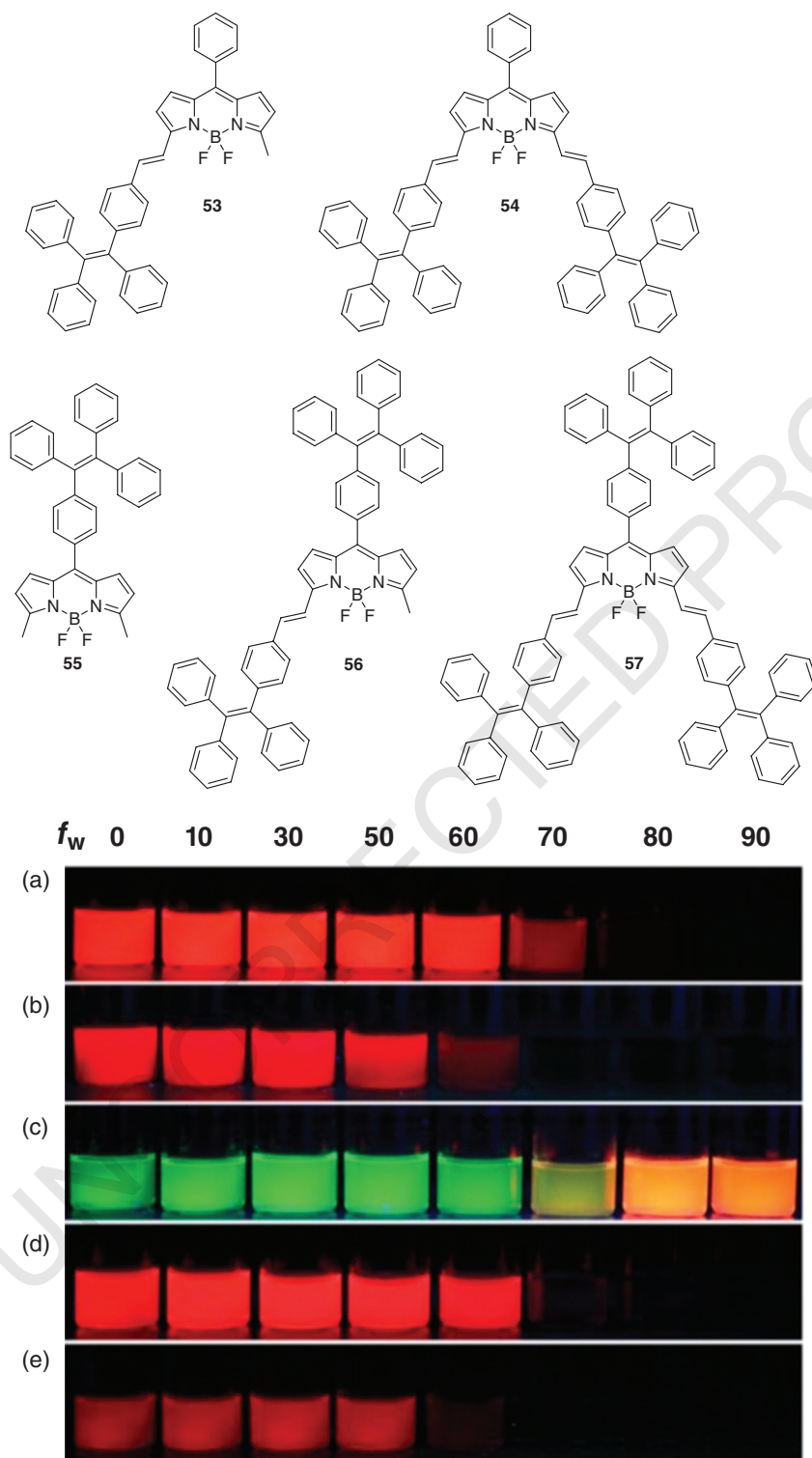


**Figure 18.13** Chemical structures of **53–57**. Fluorescence photographs of (a) **53**, (b) **54**, (c) **55**, (d) **56**, and (e) **57** in THF/water mixtures with different water fractions ( $f_w$ ) taken under UV illumination. Source: Reproduced from Ref. [71]. Copyright 2015 American Chemical Society.

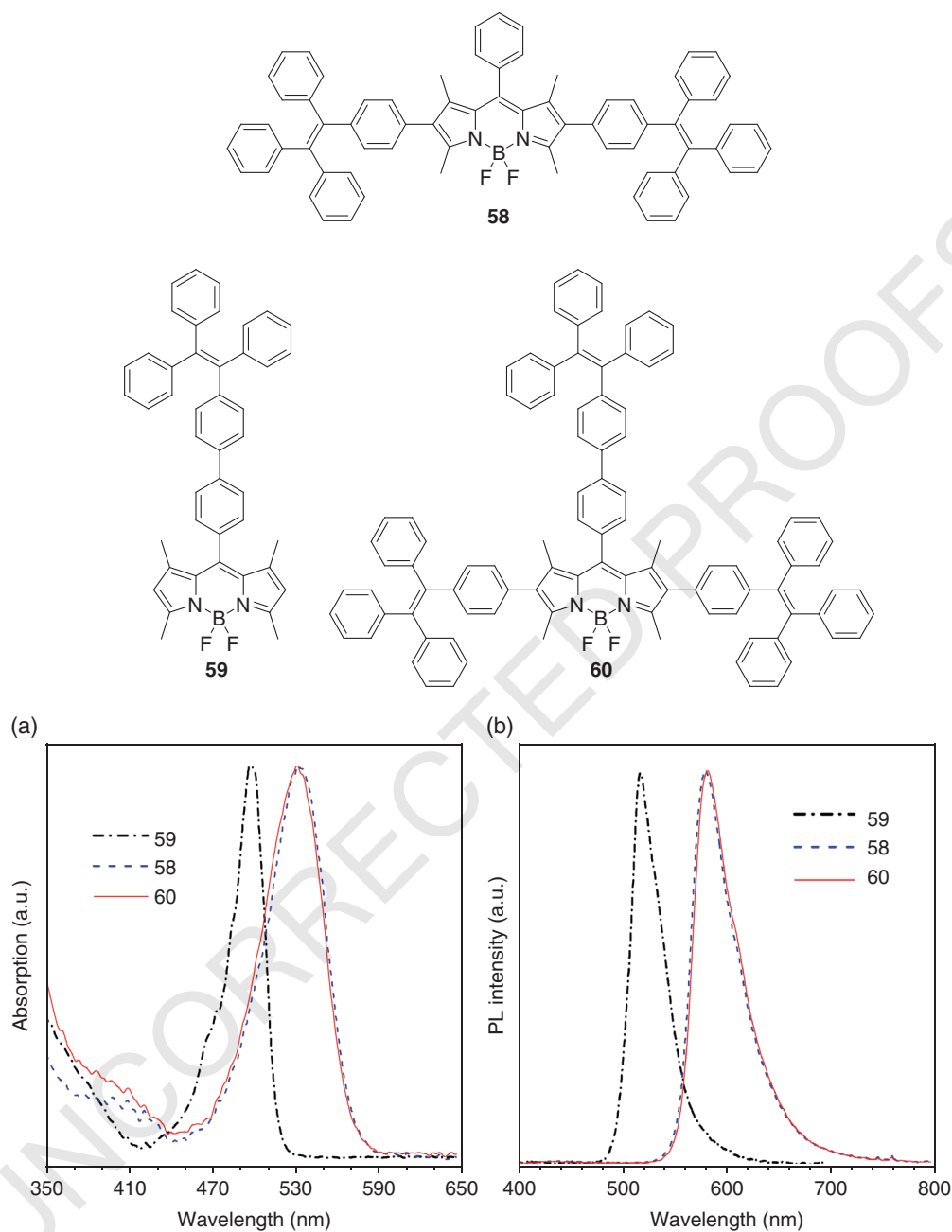


**Figure 18.14** Chemical structures of **58**, **59** and **60**. (a) Absorption and (b) photoluminescence spectra of TPE-decorated BODIPY luminogens (**58**, **59**, **60**) in dilute THF solutions. *Source:* Reproduced from Ref. [72]. Copyright 2013 Wiley-VCH Verlag GmbH & Co. KGaA, Weinheim.

Three *meso*-ester group-substituted BODIPY dyes **61–63** are also designed to investigate the influence of the position of AIE functional units TPE or triphenylethene on the BODIPY core [73]. The normalized absorption and emission spectra of **61–63** in THF solutions are shown in Figure 18.15. Compound **61** with two TPE units linked on the 3,5-positions of BODIPY core through a C=C bridge possesses absorption maximum at 673 nm and emission maximum at

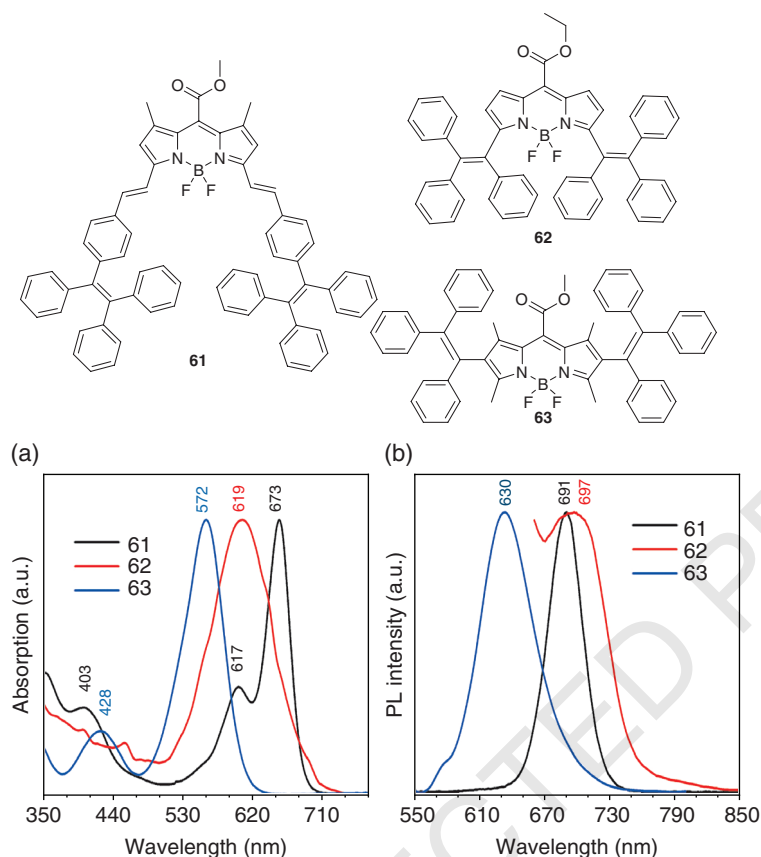


**Figure 18.15** Chemical structures of **61–63**. (a) Absorption and (b) photoluminescence spectra of **61–63** in dilute THF solutions. Source: Reproduced from Ref. [73]. Copyright 2015 Wiley-VCH Verlag GmbH & Co. KGaA, Weinheim.

691 nm with the fluorescence quantum yield of 4.7% in THF solution. When two triphenylethene moieties are directly linked on the 3,5-position of BODIPY core in **62**, the absorption maximum of THF solution is significantly blue-shifted to 619 nm, while the emission maximum does not change much and the emission efficiency increases with the fluorescence quantum yield of 6.4%. If the two triphenylethene moieties are directly linked on the 2,6-position of BODIPY core in **63**, the corresponding THF solution absorbs at 572 nm, emits at 630 nm, and its  $\Phi_F$  value is 2.9%, which is blue-shifted compared with both **61** and **62**. The thin film of **63** is emissive at 642 nm and the  $\Phi_F$  value of its crystal is 10.0%, which indicate its AIE property, while **61** shows obvious ACQ effect, suggesting that the substitution position at 3,5-site is beneficial to the elongation of the conjugation, but can easily lead to AIE-inactive. Most importantly, further functionalization and chemical modification of **63** can be conducted on the  $\alpha$ -methyl position through Knoevenagel condensation, and the ester groups on the *meso*-position of **61–63** can undergo hydrolysis to afford carbonyl acid group, which may be developed to AIE-active NIR dye for bioimaging and sensing. If the ester group in **61** is replaced to phenyl group in **64**, the compound is also ACQ, whose solution emits at 725 nm with the  $\Phi_F$  value of 78% in THF solution, which is decreased to 8% at 690 nm in the aggregated state in THF/water mixture with 80 vol% of water, owing to the good conjugation of C=C spacer linked BODIPY and TPE groups that may form a large coplanar structure and possess strong

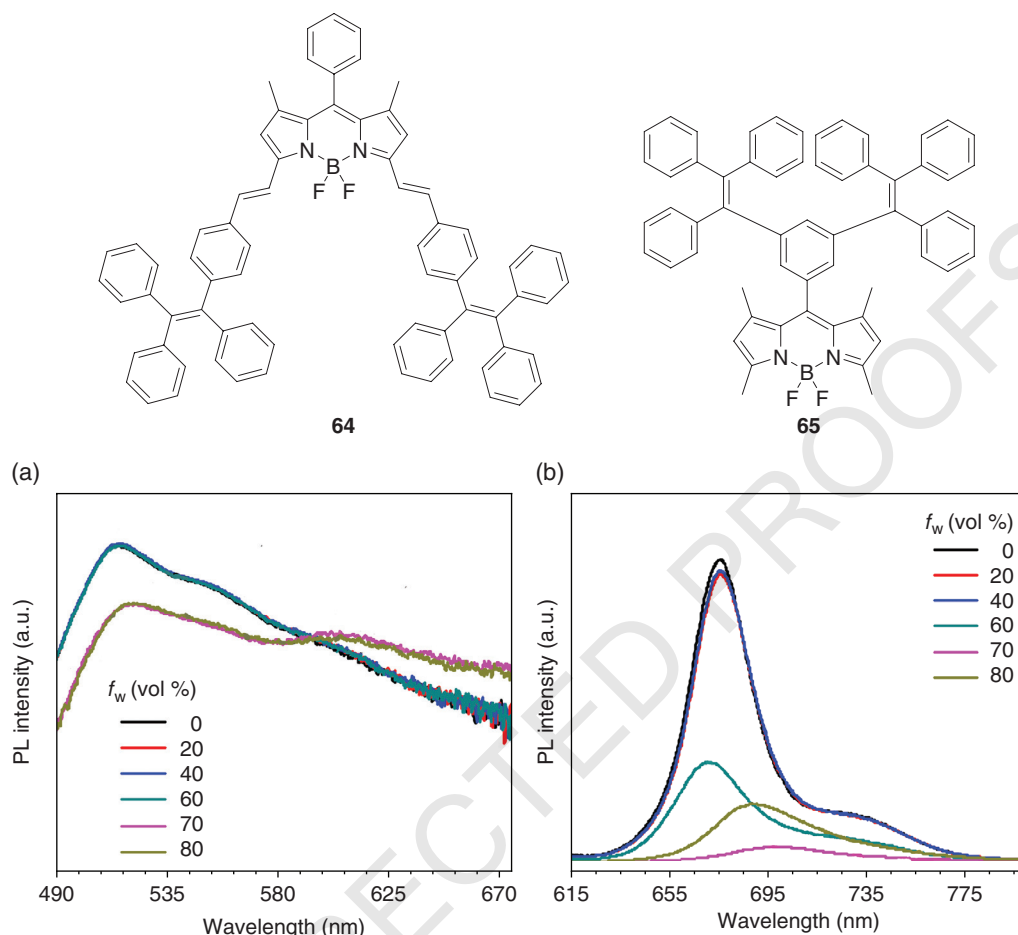


**Figure 18.16** Chemical structures of **64–65**. Photoluminescence spectra of (a) **65** and (b) **64** in THF/water mixtures with different water fractions ( $f_w$ ). Photoluminescence spectra were recorded with (a) 480 nm and (b) 600 nm excitation wavelength. Source: Reproduced from Ref. [74]. Copyright 2019 The Chemical Society Located in Taipei & Wiley-VCH Verlag GmbH & Co. KGaA, Weinheim.

intermolecular  $\pi$ – $\pi$  stacking interaction to quench the fluorescence (Figure 18.16) [74]. Compound **65** with 3,5-triphenylethene-substituted phenyl group attached on the *meso*-position of BODIPY core is also ACQ, which emits brightly in the solution state at 543 nm with the  $\Phi_F$  value of 68% and quenches to 33% in the aggregated state in THF/water mixtures with 80 vol% water content.

### 18.3.3 Substitution Group

Besides TPE-related structures, triphenylamine (TPA) units can also effectively reduce the emission quenching of D–A type fluorophores in the aggregated state, and hence it is another important functional group which can bring AIE property into BODIPY derivatives [75, 76]. The effects of substitution types and positions on the AIE property are also investigated with the emission spectra of a series of TPA–BODIPY conjugates **66–69** upon addition of different amounts of water in THF solution (Figure 18.17) [75]. Compound **66** with two TPA group attached on the 2,6-position of BODIPY core is a typical AIE-active compound: **66** shows weak red emission maximum at

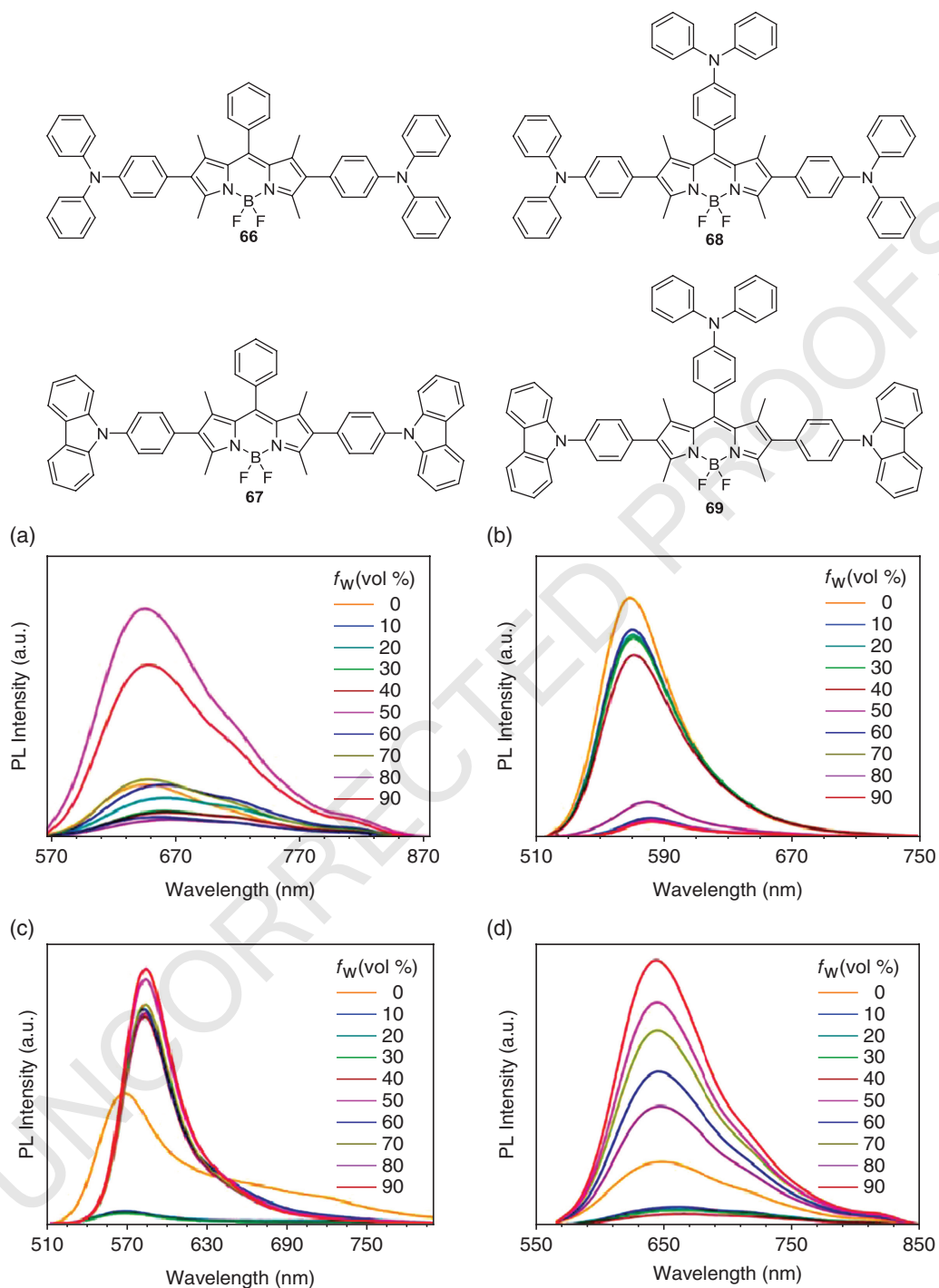


**Figure 18.17** Chemical structures of **66–69**. Photoluminescence spectra of (a) **66** (b) **67** (c) **69** and (d) **68** in THF/water mixtures with different volume fractions of water ( $f_w$ ). Source: Reproduced from Ref. [75]. Copyright 2019 American Chemical Society.

645 nm with a low-fluorescence quantum yield of 7% in THF solution. Upon addition of poor solvent, the fluorescence intensity of **66** gradually increases and the  $\Phi_F$  reaches 23% in THF/water mixture with 90 vol% of water. When the two TPA groups are replaced by *N*-phenyl carbazole moieties in compound **67**, it becomes ACQ which may be because of the existence of planar carbazole that reduces the intramolecular motion and energy loss in solution, indicating that the introduction of TPA units is crucial to convert BODIPY to AIE-active. To verify the role of TPA group, an additional TPA moiety is introduced at the *meso*-position of **67** to afford **69**, which has successfully turned the compound to AIE-active. The THF solution of **69** emits intense fluorescence at 571 nm with a relatively high-quantum efficiency of 15%. When water content in the THF/water mixture increases, emission intensity of **69** is first weakened in the presence of less than 30 vol% water fractions, then the emission intensity at 586 nm is increased gradually to reach the highest level in the presence of 90 vol% water with the  $\Phi_F$  value of 18%. Furthermore, compound **68** with three TPA units is a typical AIE compound that emits faintly at 649 nm and the emission is intensified upon the addition of water, proving that the introduction of TPA units is beneficial to AIE property. In solid state, the fluorescence quantum yields of these compounds are 22% (**66**), 13% (**67**), 24% (**68**), and 30% (**69**), respectively.

Moreover, three different functionalized TPA group bearing BODIPYs **70–72** are compared with a reference compound **73** (Figure 18.18) [76]. The THF solutions of compounds **70–73** possess similar absorption maxima at about 501 nm and emission maxima at about 517 nm, which possess small

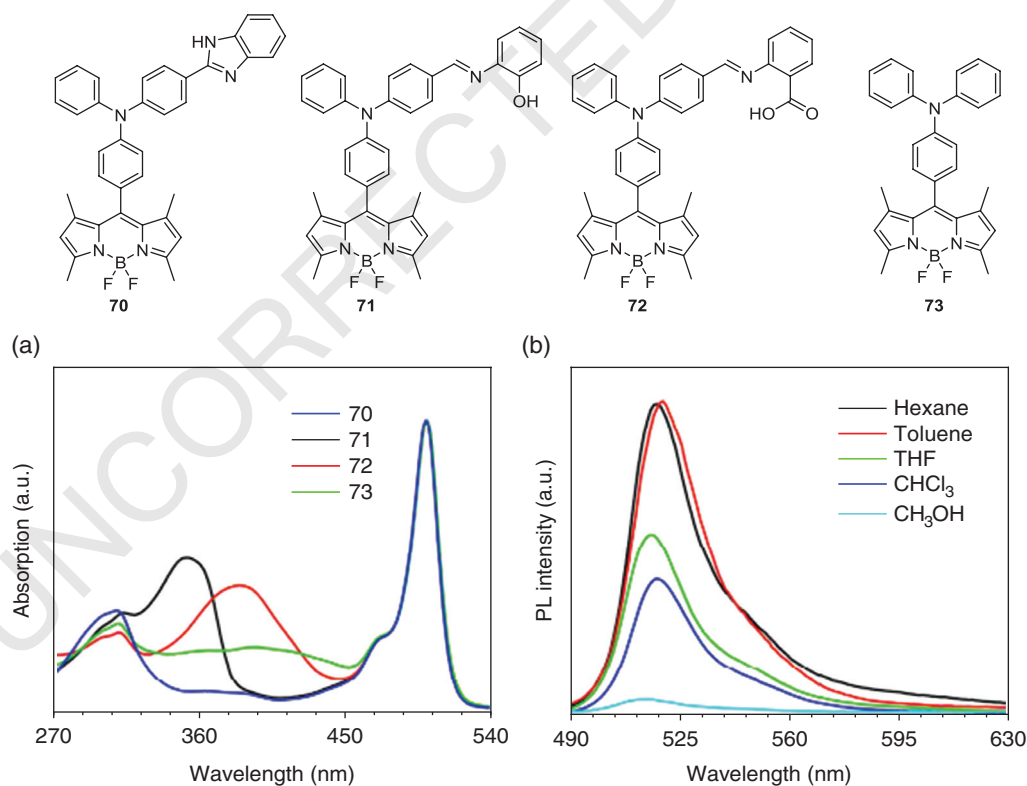


**Figure 18.18** Chemical structures of **70–73**. (a) UV absorption spectrum for **70–73** in THF. (b) Photoluminescence spectrum of **72** at the concentration of  $1 \times 10^{-5}$  M in different solvents. Source: Reproduced from Ref. [76]. Copyright 2015 Elsevier Ltd.

electronic coupling between the TPA donor and BODIPY acceptor in both the ground state and excited state. Although these TPA-BODIPY derivatives exhibit similar photophysical properties in solution, their emission behaviors in the solid state show significant difference owing to the different intermolecular interactions and molecular packing associated with the diverse TPA modifications. Compounds **70** and **71** only show weak AIE effect and upon the addition of large amount of water into their THF solution, a new weak emission peak appears at 600 nm but with very little fluorescence enhancement. On the contrary, when more than 60 vol% water is added into the THF solution of **72**, the emission maximum is red-shifted to 631 nm, accompanying with significantly enhanced fluorescence intensity. With the restriction of intramolecular twisting motions and charge transfer between TPA and BODIPY moieties, compounds **72** and **73** exhibit obvious aggregation- and crystallization-induced emission effect, which possesses high absolute fluorescent quantum yields of 12.30 and 19.47% in their crystalline states, respectively, in comparison with the values of **70** (1.37%) and **71** (3.40%). The emission behavior of these compounds in the crystalline states highly depends on the existence of the  $\pi$ - $\pi$  stacking interaction between two neighboring BODIPY fluorophores. With the cooperation of the intermolecular N-H...F or O-H...F hydrogen bonding in the crystals of compounds **70** or **71**, respectively, the dimeric structures of these two compounds show a partial or strong face-to-face  $\pi$ - $\pi$  interaction between two parallel BODIPY fluorophores, which only show weak AIE effect. On the other hand, in the crystalline states of **72** and **73**, there is no effective face-to-face  $\pi$ - $\pi$  stacking interaction between BODIPY luminophores observed.

### 18.3.4 Alkyl Substitutes on BODIPY Core

The number and position of alkyl groups substituted on the BODIPY core such as methyl group may also affect the photoluminescence behavior of the luminophores. A BODIPY-TPE derivative **7** is reported with a TPE unit directly linked on the 8-position of BODIPY core. Based on the structure of **7**, two methyl groups are attached on the 3,5-position of BODIPY in compound **55** and two methyl groups are attached on the 1,3,5,7-positions of BODIPY in compound **74** (Figure 18.19) [33]. Compound **7** without any methyl group possesses a LE state emission peak at 524 nm and a TICT state emission peak at 630 nm in THF solution. The addition of small amount of water into the solution leads to emission quenching of both peaks, however, after more than 90 vol% water is added, the peak intensity at 630 nm almost doubles, while the emission peak at 524 nm disappears, suggesting that the TICT state emission of **7** is AIE-active (Figure 18.19a). Similar phenomenon is observed for compound **55** with two methyl groups at 3,5-position of BODIPY, but the fluorescence enhancement of TICT peak is much weaker compared with that of **7** (Figure 18.19b). On the contrary, compound **74** with four methyl groups only possesses an ACQ-active LE peak, and the TICT emission can barely be observed (Figure 18.19c). Moreover, **7** possesses TICT emission peak both in THF solution and film state, **55** possesses TICT emission only in thin film state, and **74** only has a TICT shoulder emission in the thin film state. These results suggest that the introduction of methyl groups on BODIPY core can inhibit the intramolecular charge transfer behavior. Theoretical calculation and single crystal structure of **7** further proved that effective charge transfer from TPE to BODIPY took place. It not only possesses AIE characteristics, solvatochromic properties, and a large Stokes shift over 100 nm but also shows bright-red emission in both solution and solid state.

Another class of BODIPYs with three TPE units incorporated on the 2,6,8-positions of BODIPY core and H (**76**), methyl group (**77**), and ethyl groups (**78**) substituted on the 3,5-position of BODIPY are designed to study the effect of substitution groups (Figure 18.20) [77]. Compared with the corresponding mono-TPE-substituted BODIPYs **7**, **55**, and **75**, these tri-TPE-substituted BODIPYs **76-78** show significant red-shift in the absorption and emission spectra. As introduced before, compound **7**



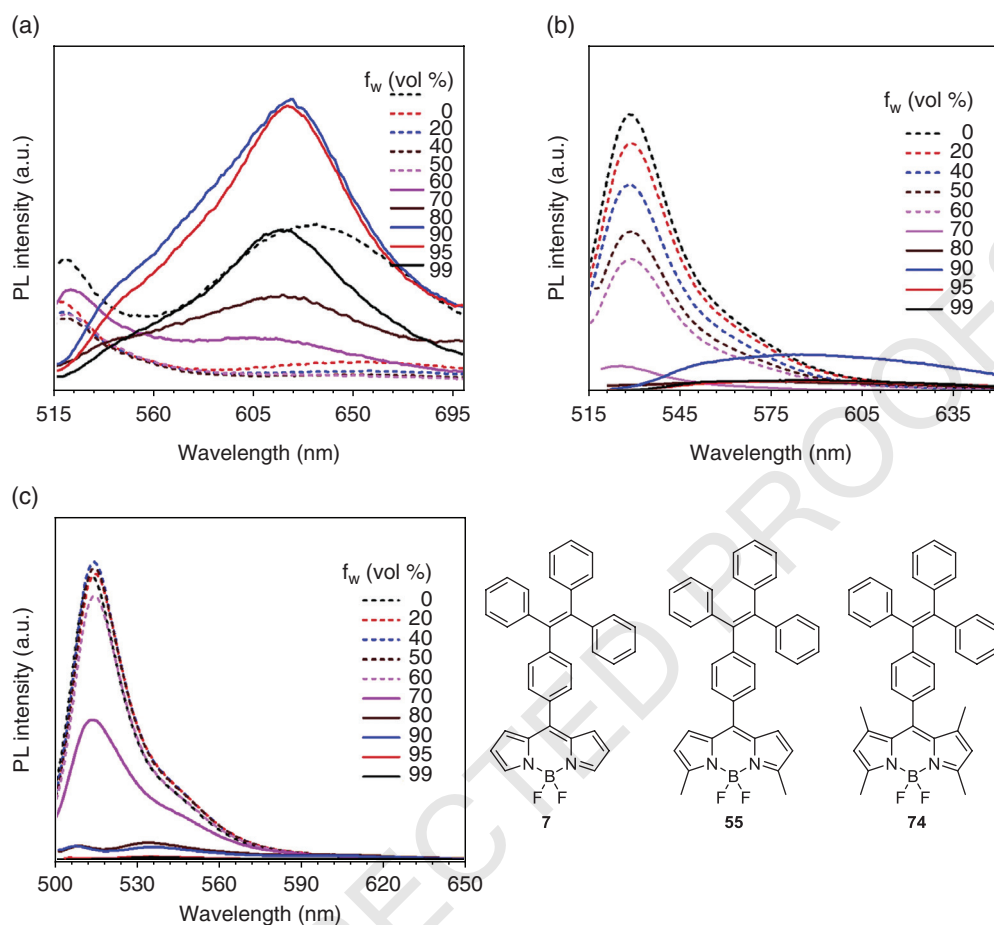


**Figure 18.19** Chemical structures of **7**, **55**, and **74**. Photoluminescence spectra of (a) **7**, (b) **55** and (c) **74** in THF/water mixtures with different water fractions ( $f_w$ ). Source: Reproduced from Ref. [33]. Copyright 2018 Elsevier B.V.

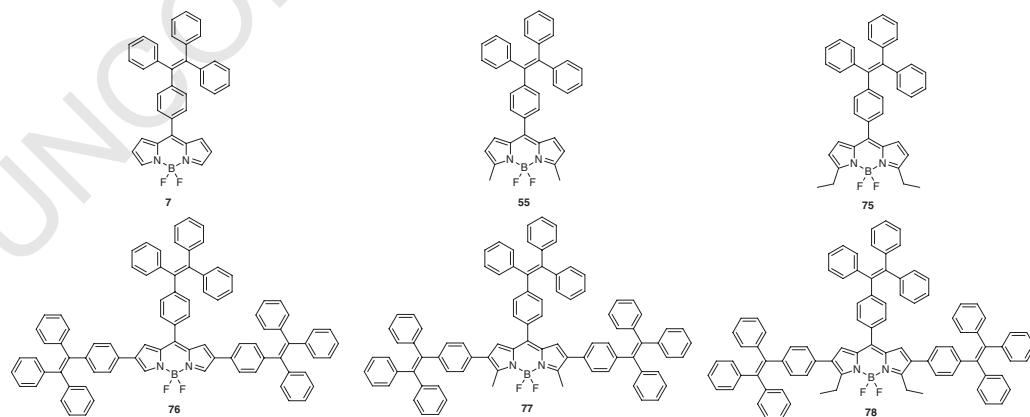


**Figure 18.20** Chemical structures of **7**, **55**, **75**–**78**. Photoluminescence spectra of (a) **76**, (b) **77**, and (c) **78** in THF/water mixtures with different water fractions ( $f_w$ ).

emits at 670 nm in THF solution, which shows an obvious AIE effect in THF/water mixtures with more than 80 vol% water. Different from that, the THF solutions of **55** and **57** possess typical BODIPY emission at about 530 nm, which gradually red-shift to 609 nm (**55**) and 640 nm (**75**) with gradual addition of water. The addition of alkyl substituents may prevent the formation of aggregates in aqueous mixtures with high water content. The THF solutions of **76–78** emit at 689, 646, and 648 nm, respectively. With gradual addition of water in the THF/water mixture, their emission intensity generally first decreases with less than 50 vol% water content, which then increases to reach maxima in 90 vol% aqueous mixture, and further increased to 1.40–1.53 times compared with that in THF solutions. In general, the addition of two TPE units have caused a more pronounced AIE effect, owing to the increased number of rotors compared with the mono-TPE-substituted BODIPYs. Notably, the  $\Phi_F$  values of thin films obtained from THF solutions of **77** and **78** have reached 68 and 98%, respectively.

### 18.3.5 AIEgens Attached Through Nonconjugated Spacers

Except the abovementioned conjugated spacer between BODIPY and TPE/TPA, these electron acceptors and donors could also be connected through nonconjugated spacers to build energy transfer systems with fluorescence resonance energy transfer (FRET) or dark resonance energy transfer (DRET) processes involved. FRET is a process that describes energy transfer between an excited-state donor fluorophore and a ground-state acceptor fluorophore linked together by a nonconjugated spacer [78]. DRET process is identical with FRET process in terms of molecular designs and energy-transfer mechanism, but differs from FRET process in that the donor moiety is non-fluorescent or weakly fluorescent, which might be called as a “dark donor” [79, 80]. For example, a series of TPE-containing BODIPYs **83–85** with one, two, or three TPE units connected to the BODIPY core through flexible alkyl chain are designed and synthesized from click chemistry [81]. The photophysical properties of these compounds are compared with their precursors **79–81** and the model compound **82** in THF solution (Figure 18.21). In these compounds, TPE groups serve as dark energy donor and BODIPY group acts as emissive energy acceptor in the DRET process, and the energy transfer efficiency of **83–85** depends on the number of TPE groups. While all the three compounds possess similar absorption maxima at 500–504 nm and emission maxima at 506–511 nm in solution, their emission efficiencies have gradually increased from 9 to 18% along with the increasing number of TPE groups in THF solution. In THF/water mixtures with 98 vol% water content, high emission intensity at 511 nm and large pseudo-Stokes shifts about 193 nm are observed when compound **85** is excited with 315 nm light, which is associated with the FRET process; while in THF solution where TPE group serves as a nonemissive dark donor; similar strong emission and large pseudo-Stokes shift are recorded owing to the DRET process. Therefore, two energy-transfer processes have been combined in these molecules to give high fluorescence with large pseudo-Stokes shifts in both solution and aggregated states.

Similarly, a series of diphenylacrylonitrile-containing BODIPYs with one, two, or three AIE units attached on BODIPY structure through flexible chain are reported, and the energy transfer process between diphenylacrylonitrile and BODIPY are studied in solvents with different polarities (Figure 18.22), suggesting that two energy-transfer processes FRET and DRET are responsible for the fluorescence enhancement of diphenylacrylonitrile-connected BODIPY compared with compounds **86–89** [82]. The comparison of photoluminescence spectra of **90–92** with their precursors **86–89** in THF solutions suggests that the strong emission at about 520 nm observed under the excitation with the absorption maximum of diphenylacrylonitrile chromophore at 330 nm is attributed to the DRET process from the dark donor of diphenylacrylonitrile moiety to the emissive acceptor BODIPY moiety. When water is added into the THF solution, the fluorescence intensity is

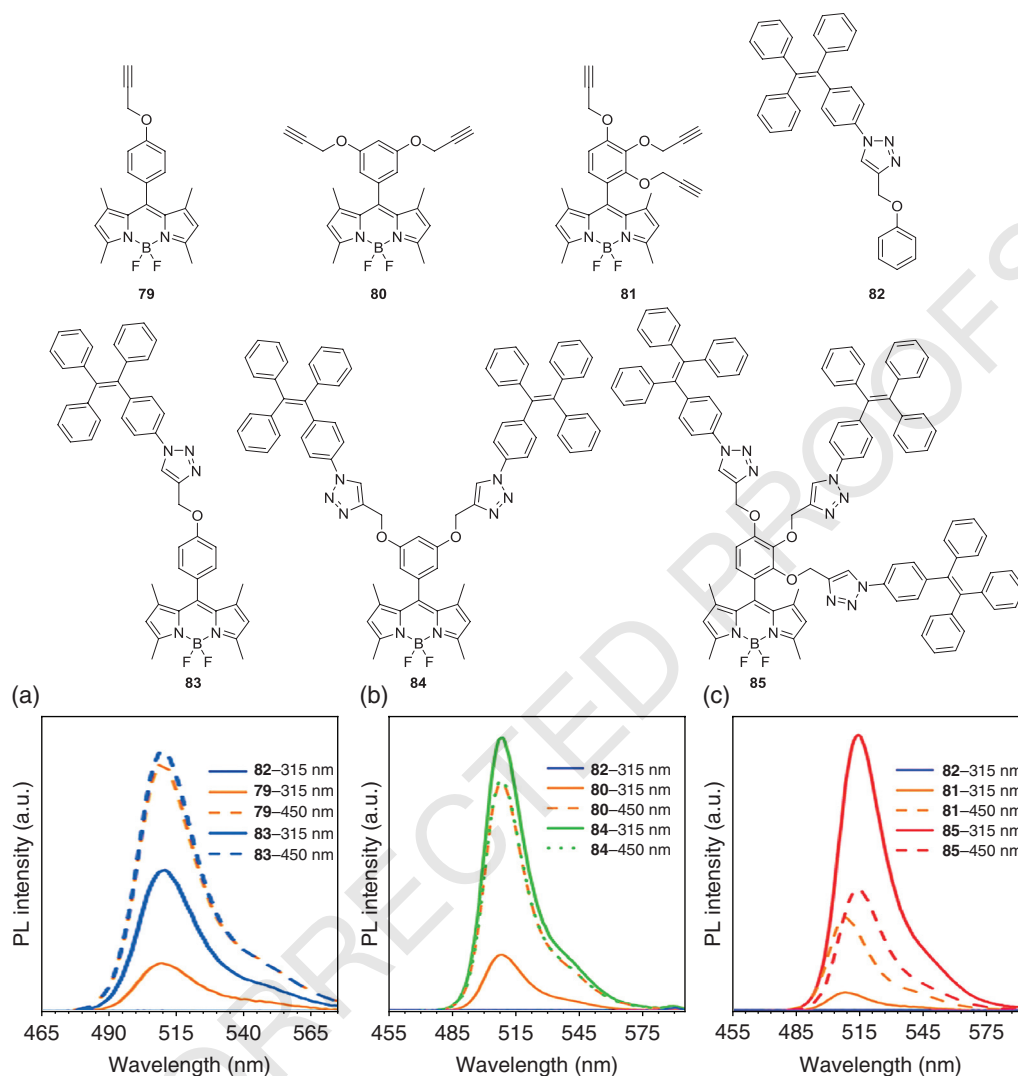


**Figure 18.21** Chemical structures of **79–85**. Photoluminescence spectra in THF solution of (a) **82**, **79**, and **83**; (b) **82**, **80**, and **84**; (c) **82**, **81**, and **85**. Source: Reproduced from Ref. [81]. Copyright 2016 Wiley-VCH Verlag GmbH & Co. KGaA, Weinheim.

enhanced with increasing amount of water, suggesting the FRET process between these two chromophores. The pseudo-Stokes shift for both DRET and FRET processes is 190 nm. Increasing the number of diphenylacrylonitrile moieties from **90** to **92** results in improved fluorescence quantum efficiency.

### 18.3.6 Other Substitution Structures

Other AIE-active BODIPYs without typical AIEgens have also been reported. For example, three thioether group-containing quinoline-based BODIPYs with different substituents ( $-\text{H}$ ,  $-\text{CH}_3$ , or  $-\text{OCH}_3$ ) **94–96** are studied (Figure 18.23) [83]. A reference compound **93** with similar structure but a chloro substitute is also studied which is not AIE-active. When Cl is replaced by thioether

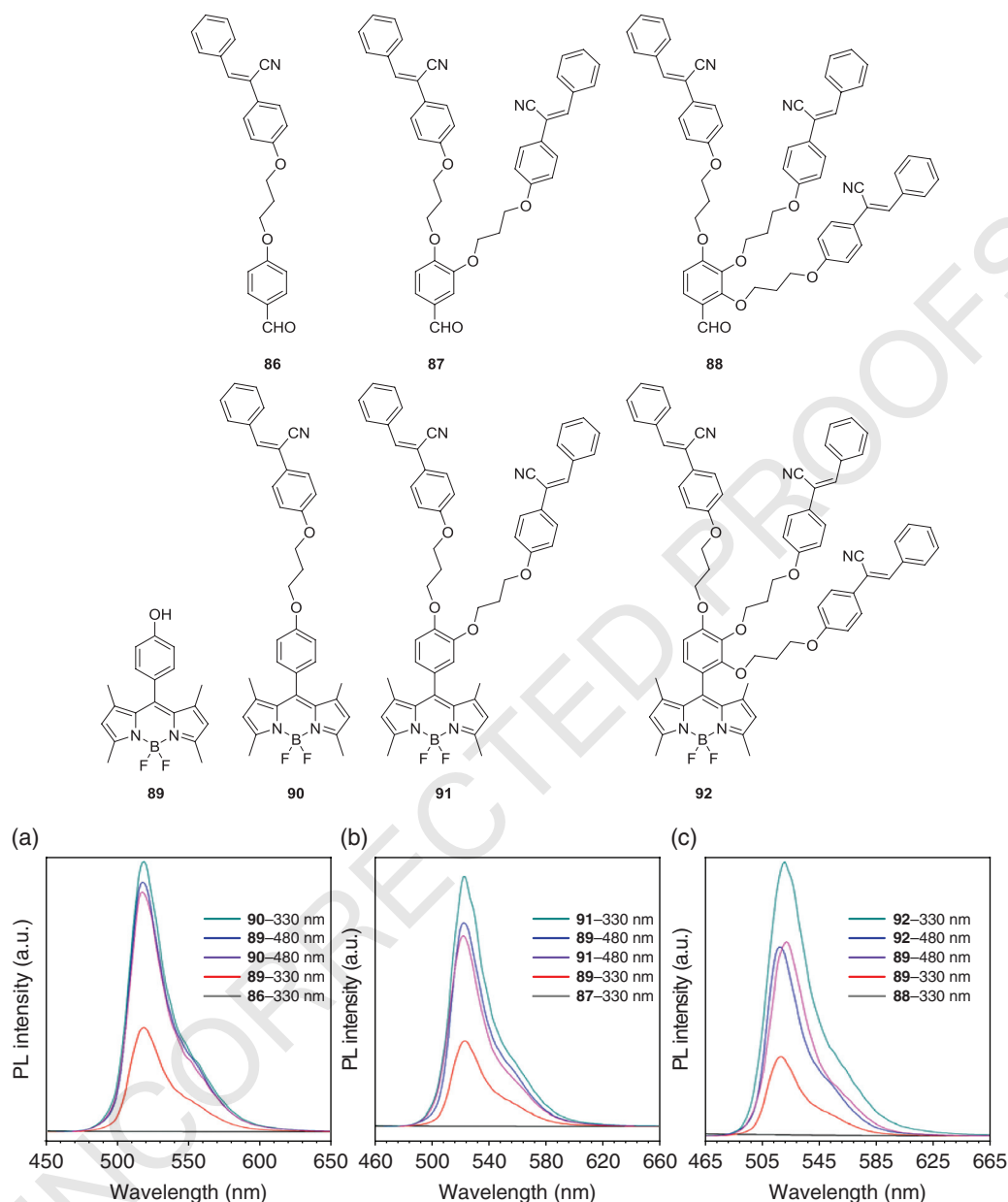


**Figure 18.22** Chemical structures of **86–92**, Photoluminescence spectra in  $1 \times 10^{-5}$  M THF solution of (a) **86**, **89**, and **90**; (b) **87**, **89**, and **91**; and (c) **88**, **89**, and **92**. Source: Reproduced from Ref. [82]. Copyright 2017 Royal Society of Chemistry.

group with larger steric hindrance, the intramolecular rotation of quinoline unit can be better restricted. Compounds **94–96** exhibit almost identical absorption maxima at  $\sim 507$  nm and emission maxima at  $\sim 530$  nm in methanol solution, and they show similar response toward addition of water. When more than 70 vol% water is added into the methanol solution, the original emissions at  $\sim 530$  nm are quenched, while new emission peaks emerge at about 571 and 612 nm. With the addition of 90 vol% water, a decrease in absorbance of compounds **94–96** is observed along with a

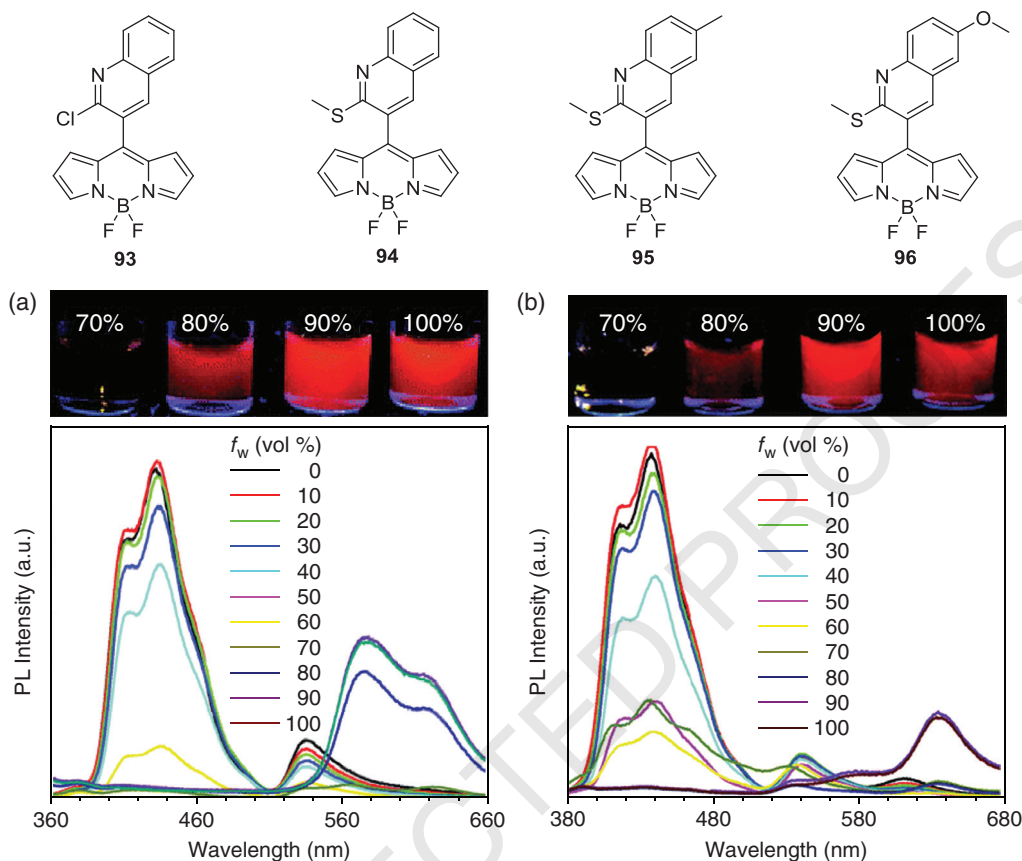


**Figure 18.23** Chemical structures of **93**–**96**. Fluorescence spectra of (a) **95** and (b) **96** in methanol/water mixture with different volume fractions of water ( $f_w$ ). Source: Reproduced from Ref. [83]. Copyright 2012 Royal Society of Chemistry.

level-off tail in the visible region and the solution color turns from yellow to red, probably attributed to the formation of nanoaggregates. The nanoaggregate morphologies can be tuned from nanoballs in **94** and **95** to reticulated nanofibers in **96**.

Last but not least, the introduction of AIEgen into BODIPY derivatives cannot guarantee AIE property of the resultant compounds [84]. For example, a series of triphenylacrylonitrile or TPE-containing BODIPYs **99**–**101**, and 4-ethynylbenzonitrile substituted BODIPY **98** are synthesized through Pd-catalyzed Sonogashira cross-coupling reaction, resulting in C≡C bond bridged AIE moiety and bare BODIPY structures (Figure 18.24). The planarization-induced extensive  $\pi$ – $\pi$  stacking and strong D–A interaction result strong fluorescence quenching in the aggregated states, and none of these compounds is AIE-active. In general, compared with model compound **97**, the installation of electron-donating group at the *meso*-position of BODIPY results in hypsochromically shifted absorption and emission spectra, while the incorporation of electron withdrawing group at the position results in bathochromically shifted absorption and emission spectra. The fluorescence quantum yields of triphenylacrylonitrile-substituted BODIPYs **99** and **100** are higher than TPE-substituted BODIPY **101**, indicating that the cyano group has minimized the CT interaction and hence increased the emission efficiency.

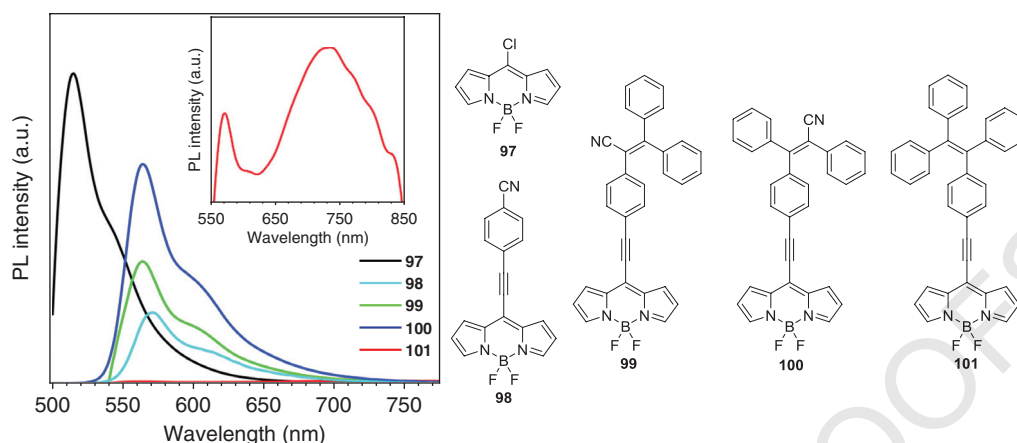


**Figure 18.24** Chemical structures of **97–101**. Photoluminescence spectra of **97–101** in THF. (Inset shows enlarged view of emission spectra of **101**). *Source:* Reproduced from Ref. [84]. Copyright 2015 American Chemical Society.

## 18.4 Application

With the unique structure and photophysical property of BODIPY derivatives, they have found a series of practical applications, and the examples as chemosensor and bioprobe are discussed in the later sections.

### 18.4.1 Chemosensor

AQ7

The electron donor/acceptor structure of most BODIPY derivatives have endowed the compounds susceptible nature which are sensitive to a range of different external stimuli, and are reflected on the emission behavior to furnish fluorescence sensors.

For example, two phenothiazine moiety-containing BODIPY derivative **44** with strong electron donor and acceptor structure is reported to exhibit multistimuli responsive characteristics, including grinding, organic solvent, acid or base vapors (Figure 18.25a) [64]. The THF solution of **44** absorbs at 440 nm and emits at 473 nm with a  $\Phi_F$  value of 12%. The yellow solid powder of **44** possesses intense emission at 540 nm upon UV irradiation, which is switched to an orange powder with red emission at 635 nm after simple grinding. The color and emission of the ground powder of **44** are recovered after further exposure to  $\text{CH}_2\text{Cl}_2$  vapor, demonstrating the reversibility of the piezochromic effect of **44**. With the protonation–deprotonation affected structure and luminescence, together with the mechanofluorochromism property of **44**, a simple, convenient, and efficient technology for information encryption and decryption is designed (Figure 18.25b). In the encryption stage, the “writing” information is hidden by tartrazine and cannot be observed either under ambient light or under UV light, while in the decryption stage, the yellow fluorescence of the characters “ZHJ” can be revealed clearly after exposing the test paper to triethylamine vapor for 10 minutes. These features have enabled the potential application of this BODIPY derivative in fluorescence sensing, detection, and security protection.

Besides mechanical force, the emission behavior of BODIPY derivatives is also sensitive to viscosity and temperature. For example, compound **21** with two BODIPY moieties linked on each end of benzodithiophene core is found to possess various excited-state conformations which may lead



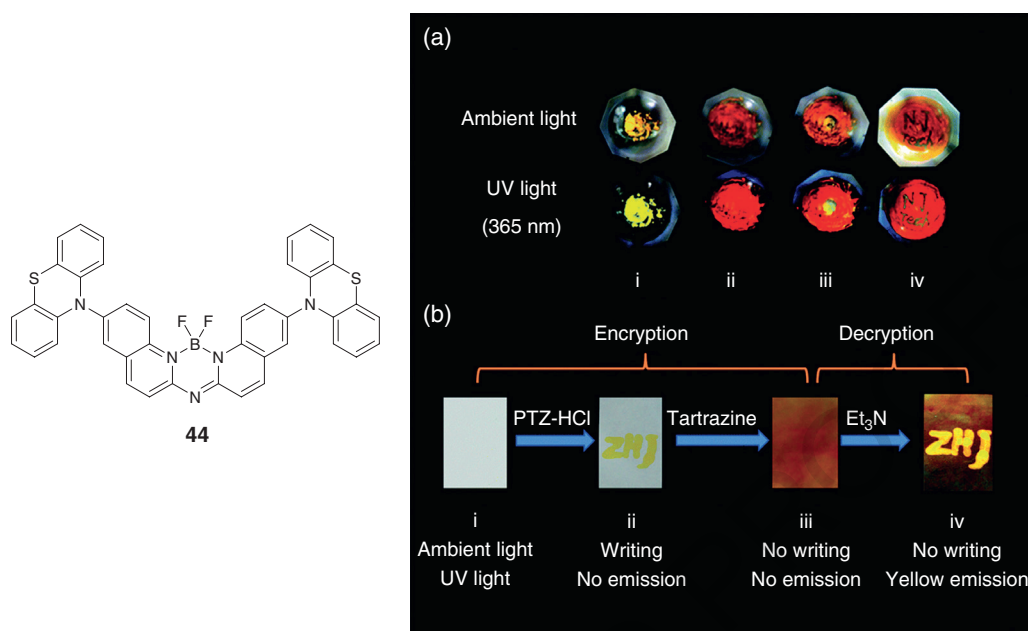


**Figure 18.25** (a) Photographic images of **44** in response to mechanical grinding under irradiation of ambient light and UV light at 365 nm; (b) photographic images of information encryption and decryption. Source: Reproduced from Ref. [64]. Copyright 2014 Royal Society of Chemistry.

to viscosity-dependent emission (Figure 18.26) [45]. Restricting the rotation of molecular rotors in viscous media such as a series of methanol and glycerol mixtures enhances fluorescence intensity. Increasing the ratio of glycerol in the mixed solution, both solvent polarity and viscosity are increased. While the former generally lead to red-shifted and quenches emission, the latter is dominant which usually restricts the intramolecular rotation and thereby leads to enhanced locally excited emission at about 425 nm exclusively. Furthermore, the temperature-dependent fluorescence of compound **21** is measured in THF solution, suggesting that the emission of **21** is highly sensitive to temperature. When the solvent temperature is increased from -20 to 50 °C, the TICT emission band is gradually blue-shifted from about 660 to 645 nm with significantly raised emission intensity. The readily tunable emission of **21** in the red region and prominent viscosity- and temperature-sensitive emission endow the compound as promising ratiometric viscosity and temperature sensor.

BODIPY derivatives with proton donor or acceptor commonly possess pH-dependent emission which can hence be developed as pH sensors. For instance, TPA-containing BODIPY **72** with *o*-carboxyl-benzoylhydrazone is reported as a solid-state fluorescence detector for HCl vapor with high stability and emission efficiency (Figure 18.27) [76]. The emission of thin film of **72** is monitored upon exposure to air, suggesting that it's high photostability after exposure to air for one week. However, upon exposure to HCl vapor for 10 minutes, the emission of **72** is quenched by 85%, probably because the binding of HCl with **72** through the protonation of the imine group in addition to the N atom from TPA moiety may promote the intramolecular twisting motion with concomitant change of the molecular packing in the thin film state and the TICT process, which caused the fluorescence quenching. The single crystal of **72** emits at 570 and 632 nm with the  $\Phi_f$  value of 12.3%. After fuming with HCl vapor for 10 minutes, the emission at 570 nm almost



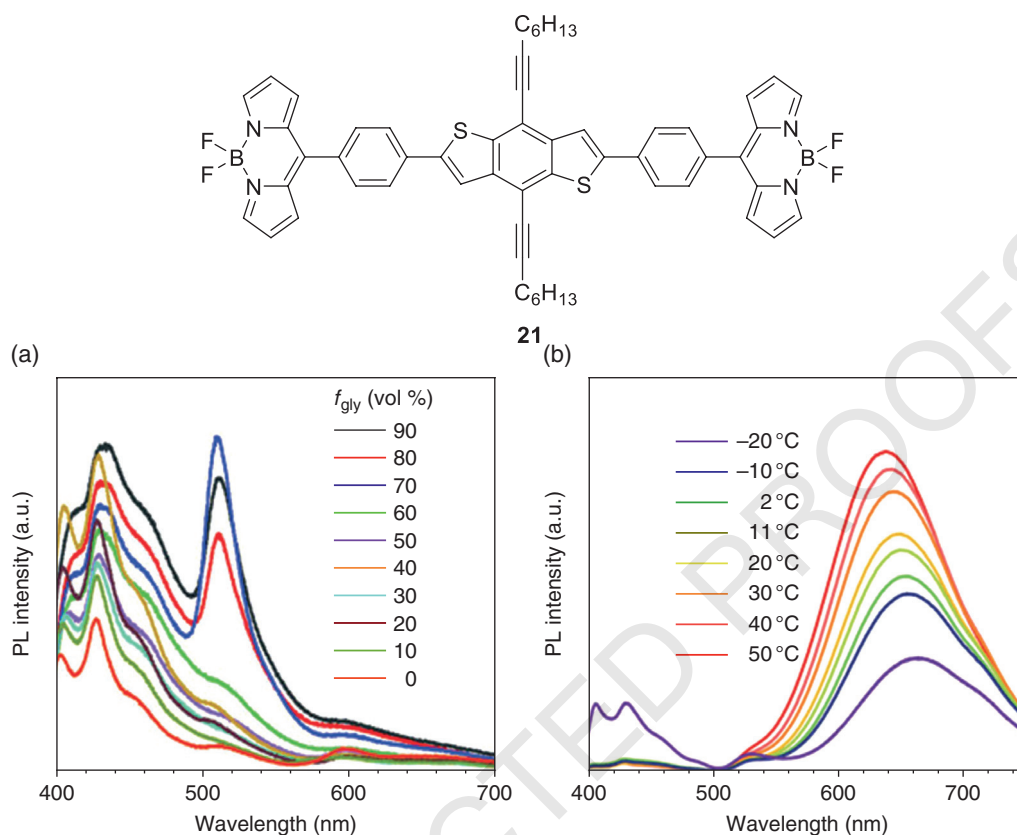
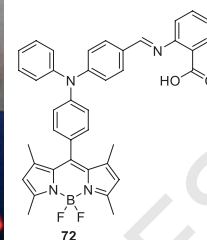



**Figure 18.26** (a) Viscosity-dependent fluorescence emission spectra of **21** in glycerol/methanol mixtures with different glycerol fractions ( $f_{gly}$ ); (b) temperature-dependent fluorescence emission spectra of **21** in THF. Source: Reproduced from Ref. [45]. Copyright 2019 Wiley-VCH Verlag GmbH & Co. KGaA, Weinheim.

disappears and the emission at 632 nm also decreases. The fast fluorescence “on-off” response toward HCl vapor has made the compound desirable solid-state-fluorescent sensor for acidic vapor detection.

With the unique structure of BODIPY core, a few analytes are expected to have strong interaction with boron site and bring influence on the emission behavior of the compounds, especially nucleophilic anions such as  $F^-$  and  $CN^-$  [85]. A  $C_3$ -symmetric compound **16** with three 2-formyl BODIPY branch linked on a TPA core is reported to selectively and simultaneously detect  $F^-$  and  $CN^-$  with distinct color and fluorescence change among a series of different ions including  $Cl^-$ ,  $Br^-$ ,  $I^-$ ,  $HSO_4^-$ ,  $NO_3^-$ ,  $ClO_4^-$ ,  $NO_2^-$ ,  $S_2^-$ , and  $CO_3^{2-}$  through the decomposition of BODIPY core (Figure 18.28) [41]. Strong emission of **16** is observed at 524 nm in THF/water mixture (v/v, 98/2), and addition of  $F^-$  into the solution leads to a slight blue-shift to 519 nm and the emergence of a new emission peak at 471 nm. When 34 equivalents of  $F^-$  is added, the emission intensity at 471 nm is increased by 8.3-fold while that at 524 nm is quenched by 89%. Similar for  $CN^-$ , when 34 equivalents of  $CN^-$  is added, the emission intensity at 475 nm is increased by 20.9-fold while that at 524 nm is quenched by 94%. The preferential binding of  $F^-$  and  $CN^-$  at the boron center of BODIPY core may cause detachment of stable difluoroboron bridges in BODIPY core due to a nucleophilic substitution to break a B–N bond and generate B–F, B–C $\equiv$ N, and N–H bonds, respectively, resulting in decomposition of the fluorophore, which is responsible for the fluorescence



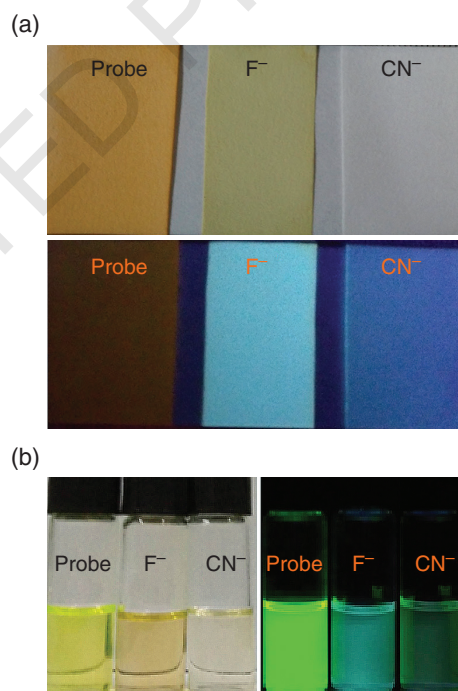
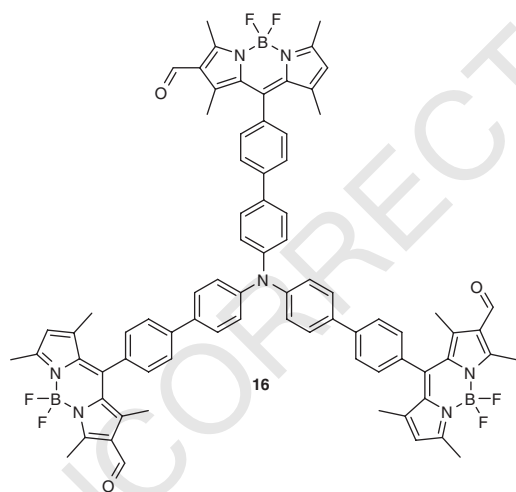

  
 film form after exposing to HCl vapor  
 g to HCl vapor under natural light (top  
 from Ref. [76]. Copyright 2015

robe       $F^-$        $CN^-$

robe       $F^-$        $CN^-$

$F^-$        $CN^-$

Probe       $F^-$        $CN^-$



detection of these two ions. Similar color and fluorescence changes are also observed in solution state. Therefore, the colorimetric and fluorometric test strip of **16** can be used to differentiate interfering cyanide and fluoride ions simultaneously in a convenient way.

### 18.4.2 Bioimaging

With the advantages of stable spectral properties, high fluorescence quantum yield, high-molar extinction coefficient, tunable emission, high photo- and chemical stability, and good biocompatibility, the major applications of BODIPY derivatives are found in biological imaging and probing.

For example, compound **40** with a pyrazoline attached on the *meso*-position of BODIPY core can self-assemble to form red-emissive nanoparticles for bioimaging (Figure 18.29) [60]. The photo-physical properties of **40** is studied in THF/*n*-hexane mixtures with different ratios, and the emission of **40** gradually changes from red to green with increasing fraction of *n*-hexane, suggesting that the LE state emission becomes dominant in such low polar mixed solution. The nanoparticles of **40** emits at 623 nm. Surprisingly, the cell-staining process with nanoparticles of **40** is ultrafast, which only takes five seconds-incubation at room temperature to observe apparent fluorescence in the cells. When the incubation time extends from five seconds to 10 minutes, the intracellular fluorescence gradually increases, indicating the nanoparticles could be continuously endocytosed and accumulated in the cytoplasm. Furthermore, long-term fluorescence signal tracking in vivo for about 12 days is also realized. The bright red fluorescence, ultrafast cell staining ability, and long-term in vivo tracking competence outline the great potential of these AIE-active BODIPY compounds for monitoring biological processes. Fluorescent nanoparticles built from AIE-active BODIPY dyes

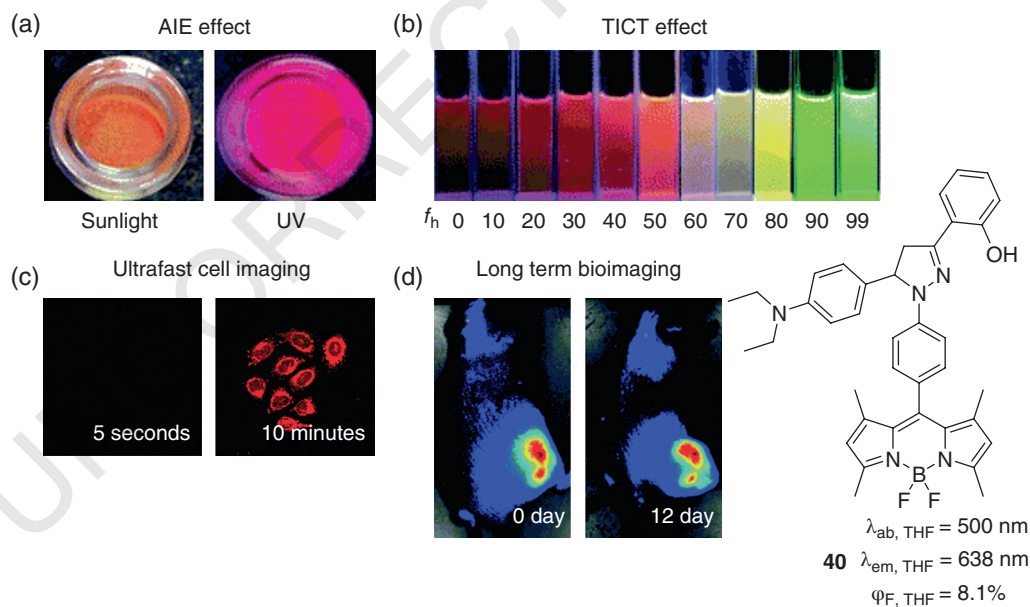


**Figure 18.29** (a) Photograph of **40** powder under sunlight and UV light. (b) The photograph of **40** at different ratios of THF/*n*-hexane under 365 nm lamp irradiation. (c) CLSM images and relative fluorescence intensity of HeLa cells incubated with the nanoparticles of **40** for different times. (d) in vivo fluorescence imaging of the nanoparticles of **40** in the anesthetized mouse performed in the Maestro 500FL in vivo optical imaging system. Source: Reproduced from Ref. [60]. Copyright 2016 Royal Society of Chemistry.

and amphipathic polymeric matrixes have also designed for long-term bioimaging [75]. The nanoparticles prepared from TPA-BODIPY derivative **68** exhibit bright red emission at 650 nm and high-fluorescence quantum yield of 26% in aqueous media, which can be internalized by HeLa cells by simply shaking the culture media with cells for about five seconds at room temperature, demonstrating an ultrafast and easy-to-operate staining protocol (Figure 18.30). Most importantly, these nanoparticles exhibit excellent long-term imaging capabilities both in vitro and in vivo for over 14 days. In another example, a deep-red-emissive TPA-BODIPY derivative **15** modified with two oxadiazole units is used for living cell imaging of MDA-MB-231 cells (Figure 18.31) [40]. The THF solution of **15** absorbs at 500 nm, while dual emissions are observed at 647 and 513 nm with the  $\Phi_F$  value of 11%, and the red emission increases with the addition of large amount of water. Compound **15** is easily internalized by MDA-MB-231 cells, and the bright red fluorescence is clearly observed from the viable cells under fluorescence microscope, suggesting no apparent toxicity of the dye. Moreover, in THF/water mixture with 90 vol% water, the fluorescence intensity of **15** is strengthened continuously with the increasing concentration of BSA to reach 4 times enhancement, indicating its function as bioprobe for BSA.

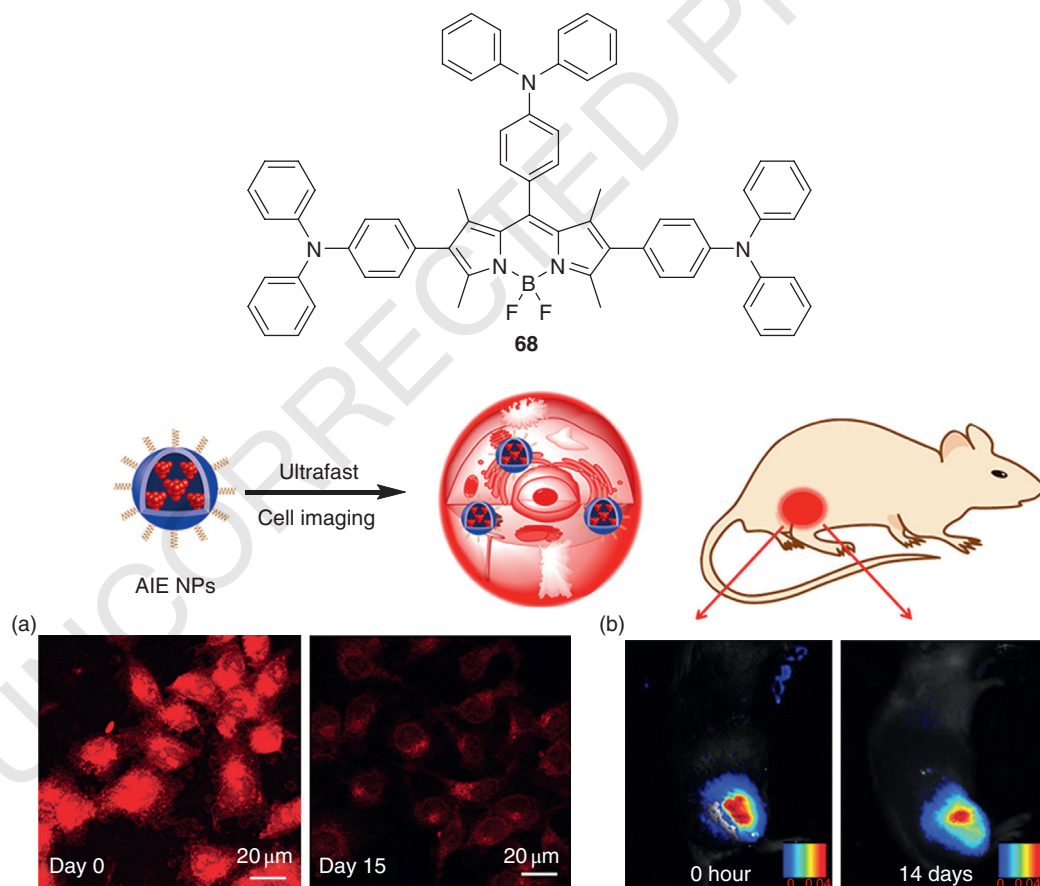


**Figure 18.30** Ultrafast and noninvasive long-term bioimaging. (a) Long-term cell tracing images of **87** nanoparticles at 37 °C for 6 hours and then subcultured for 0 and 15 day. (b) in vivo fluorescence images of the tumor-bearing mouse subcutaneously injected with **68** nanoparticles in 0 and 14 day. Source: Reproduced from Ref. [75]. Copyright 2019 American Chemical Society.

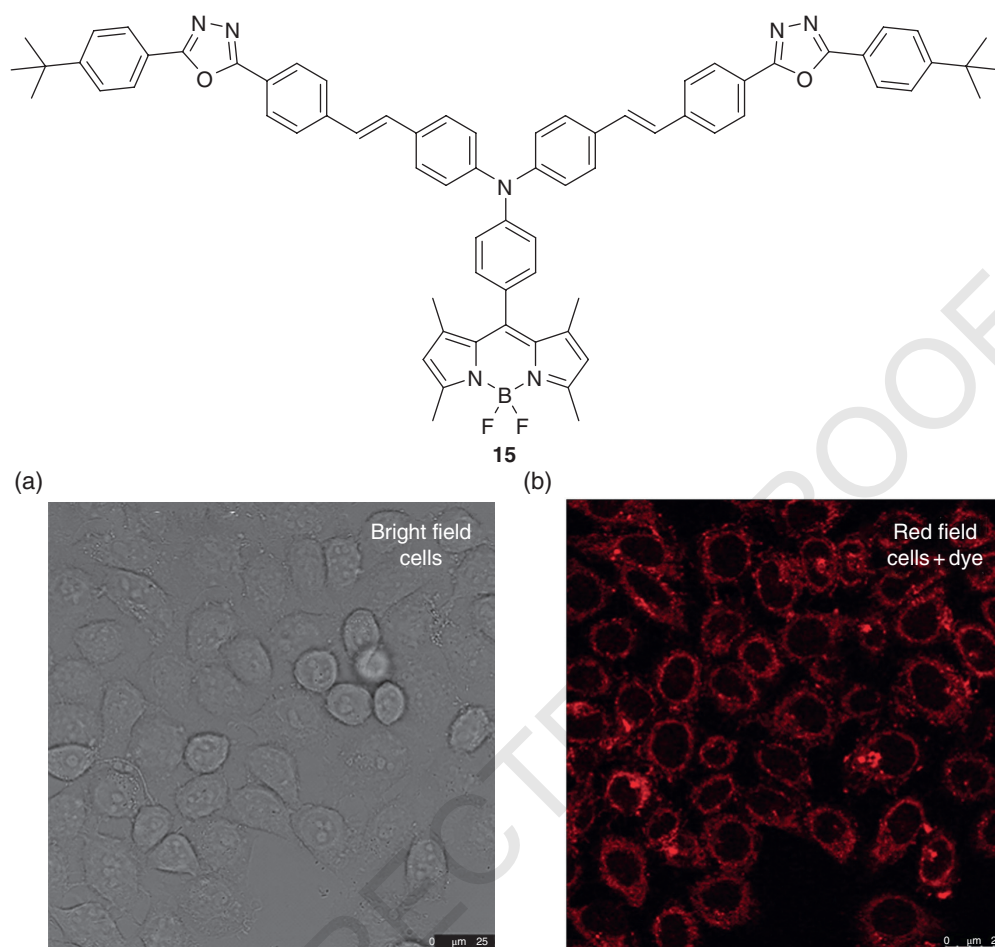


**Figure 18.31** Laser confocal fluorescence microscope photos of **15** coinubation with MDA-MB-231 cells. (a) Cells photo of **15** in bright field; (b) cells photo of **15** in red field. Laser excitation wavelength: 552 nm. Source: Reproduced from Ref. [40]. Copyright 2017 Elsevier B.V.

The intracellular pH environment could also be imaged by BODIPY dyes. For example, BODIPY **43** modified with a benzimidazole group on its 2-position is designed for ratiometric pH imaging with a dual excitation/dual emission model in A549 cells at different pH condition [63]. When the pH value is decreased from 6.5 to 3.8, the green channel images excited with 488 nm light disclosed that the intrinsic emission is enhanced, whereas the emission in red channel images excited with 543 nm light decreases gradually at the same time, suggesting the ratiometric pH-sensing ability of **43**. Synchronization of lysosome disruption with cellular acidification in the crystalline silica-induced silicosis is observed directly by costaining A549 cells with LysoTracker and **43**, which reveals that the small particle-induced cellular acidification is associated with particle size and chemical nature of the particle. Compound **43** can hence be used for imaging in cell acidification caused by crystalline silica exposure. In another example, piperazine-containing, naphthalimide-BODIPY derivative **38** is designed as pH probes for selective lysosome tracking in living cells [58]. The confocal images of HeLa cells after treatment with **38** and counter staining with LysoTracker Red DND-99 suggest that the green emission from **38** matches well with the red signal from



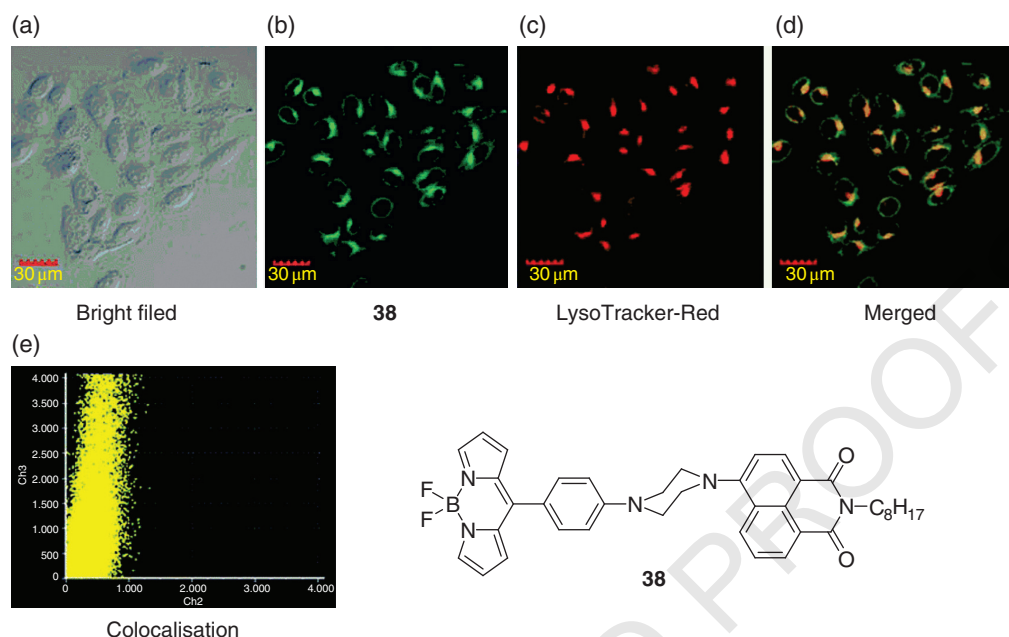


**Figure 18.32** Confocal images of HeLa cells after treatment with **38** and counter staining with "LysoTracker™ Red DND-99." *Source:* Reproduced from Ref. [58]. Copyright 2019 Royal Society of Chemistry.

LysoTracker Red (Figure 18.32). Both signals are distributed in the perinuclear region, and colocalization of the probes can be clearly seen with yellow spots in the merged image. The BODIPY probe thus shows good biocompatibility and potential of long-term monitoring of the lysosomal morphology, which may track physiological and pathological changes during various cellular processes.

Besides pH condition, BODIPYs could also be used for imaging biothiols such as cysteine (Cys), homocysteine (Hcy) and glutathione (GSH) in living cells, which have attracted extensive interest because of their vital roles in a variety of physiological processes [38]. For example, TPA-containing BODIPY compound **12** with a cyano and a bromo group attached on the TPA moiety and a *p*-aminophenylthio group located at the 3-position is used for imaging biothiols in living A549 lung cancer cells (Figure 18.33). Compound **12** is found to be nearly nonemissive. When it is treated with GSH, only a slight fluorescence enhancement is observed; however, upon treatment of Cys or Hcy, the fluorescence intensity is raised by 1081 and 1126 folds, respectively, which demonstrate good selectivity and sensitivity toward Cys and Hcy over GSH and other amino acids in a wide pH range from 2 to 10 in aqueous buffers. The fluorescence imaging behavior is also demonstrated in living A549 lung cancer cells. When A549 cells are incubated with **12** after preincubation with Cys, bright emission can be observed in both green and red channels; when the cells are pretreated with thiol-blocking agent, only weak emission can be observed. Besides exogenous biothiols, the probe can also detect endogenous biothiols in living A549 lung cancer cells.

H<sub>2</sub>S could also be detected in vivo by BODIPY dyes. A H<sub>2</sub>S-responsive BODIPY derivative **9** bearing a TPE group and a chloro atom at the 3-position has shown ratiometric fluorescence and NIR-II emission light-up upon H<sub>2</sub>S activation for in vitro and in vivo imaging (Figure 18.34) [36]. Compound **9** possesses an absorption maximum at 550 nm in Tris/CH<sub>3</sub>CN buffer solution. The good spectral overlap between the emission of TPE and absorption of BODIPY facilitates efficient



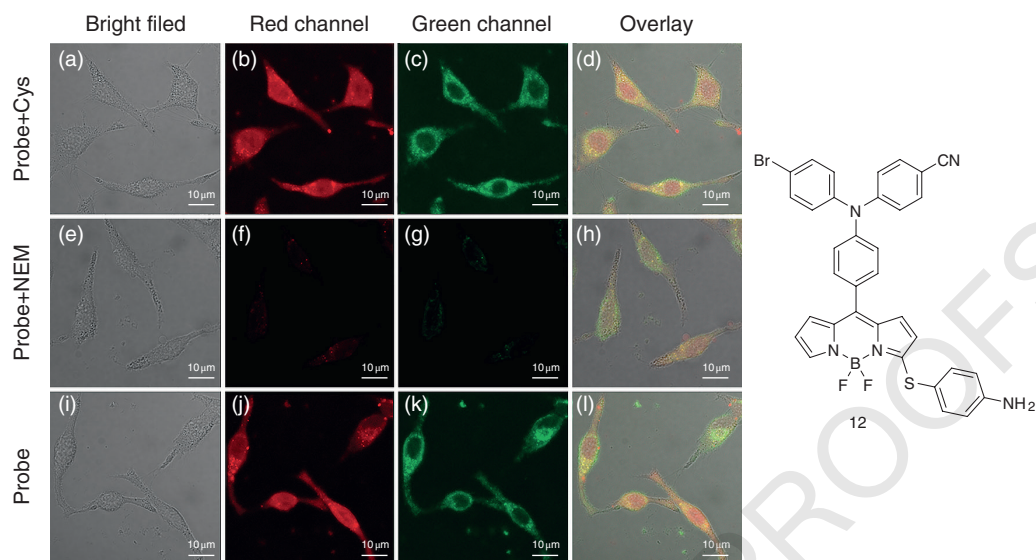


**Figure 18.33** (a–d) Confocal fluorescence and bright-field images of A549 cells incubated with probe **12** after preincubation with Cys. (e–h) Confocal fluorescence and bright-field images of A549 cells incubated with probe **12** after preincubation with *N*-ethylmaleimide (NEM). (i–l) Confocal fluorescence and bright-field images of A549 cells incubated with probe **12**. Source: Reproduced from Ref. [38]. Copyright 2017 Elsevier Ltd.

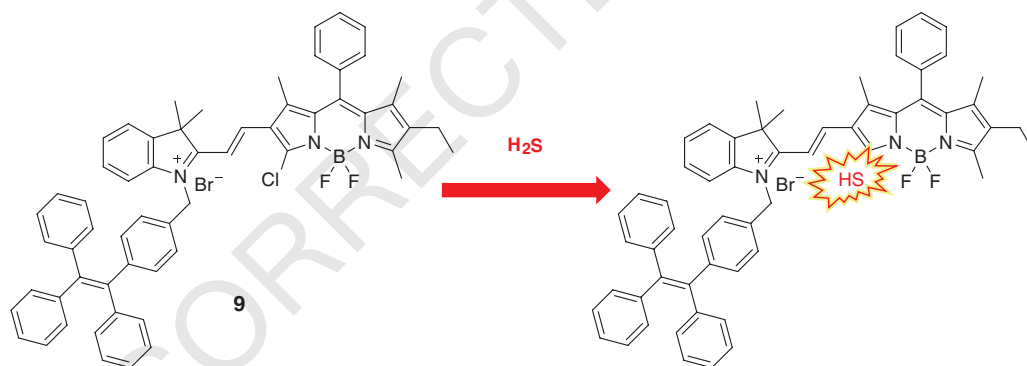


**Figure 18.34** The mechanism for  $\text{H}_2\text{S}$ -mediated radiometric, NIR fluorescence light up and their bioimaging  $\text{H}_2\text{S}$  in Living Cells. (a) HCT116 cells pretreated with AOAA followed by incubation with probe **9**. (b) HCT116 cells incubated with probe **9**. (c) HCT116 cells pretreated with SAM followed by loading with probe **9**.

FRET process to quench the emission. In the presence of  $\text{H}_2\text{S}$ , the Cl-group is substituted by HS-group, which has resulted in an obvious red-shift of the absorption spectra of BODIPY and hence attenuated the FRET process. More importantly, after being activated by  $\text{H}_2\text{S}$ , new fluorescence at new emission at 920 nm is observed from the dye, and the fluorescence tail extends to 1300 nm, indicating potential second near-infrared (NIR-II) imaging. The incubation of HCT116 cells and **9** for 30 minutes afforded a bright and stable emission signals in the blue channel and a relatively weak emission in the red channel with ratio of 2.82 : 1. When a cystathionine- $\beta$ -synthase (CBS) inhibitor, aminooxyacetic acid, is added to inhibit the  $\text{H}_2\text{S}$  production, the emission intensity ratio

from blue channel to red channel has dropped to 0.70 : 1; in contrast, when an allosteric CBS activator, *S*-adenosyl-L-methionine, is added to promote the production of  $\text{H}_2\text{S}$ , the ratio increased to 3.59 : 1. These results indicate that probe **9** can serve as a potential sensor to detect endogenous  $\text{H}_2\text{S}$  rapidly and specifically, which can potentially be used for imaging of  $\text{H}_2\text{S}$ -rich cancer cells and tumors.

Transition metal species could also be probed by AIE-active BODIPY dyes other than small molecular bio-analytes. An AIE-active BODIPY derivative **2** with an allyl ester group installed on the 8-position of BODIPY with improved water solubility is designed as a two-channel responsive probe for palladium in aqueous solution (Figure 18.35) [30]. The pink solution of **2** possesses a broad absorption peak at 516 nm and a sharp absorption peak at 587 nm, with an orange fluorescence peaked at 591 nm. After treatment with 20  $\mu\text{M}$  of  $\text{Pd}(\text{PPh}_3)_4$ , the solution color changes to yellow, the absorption peak significantly blue-shifts to 495 nm, and the emission color changes to

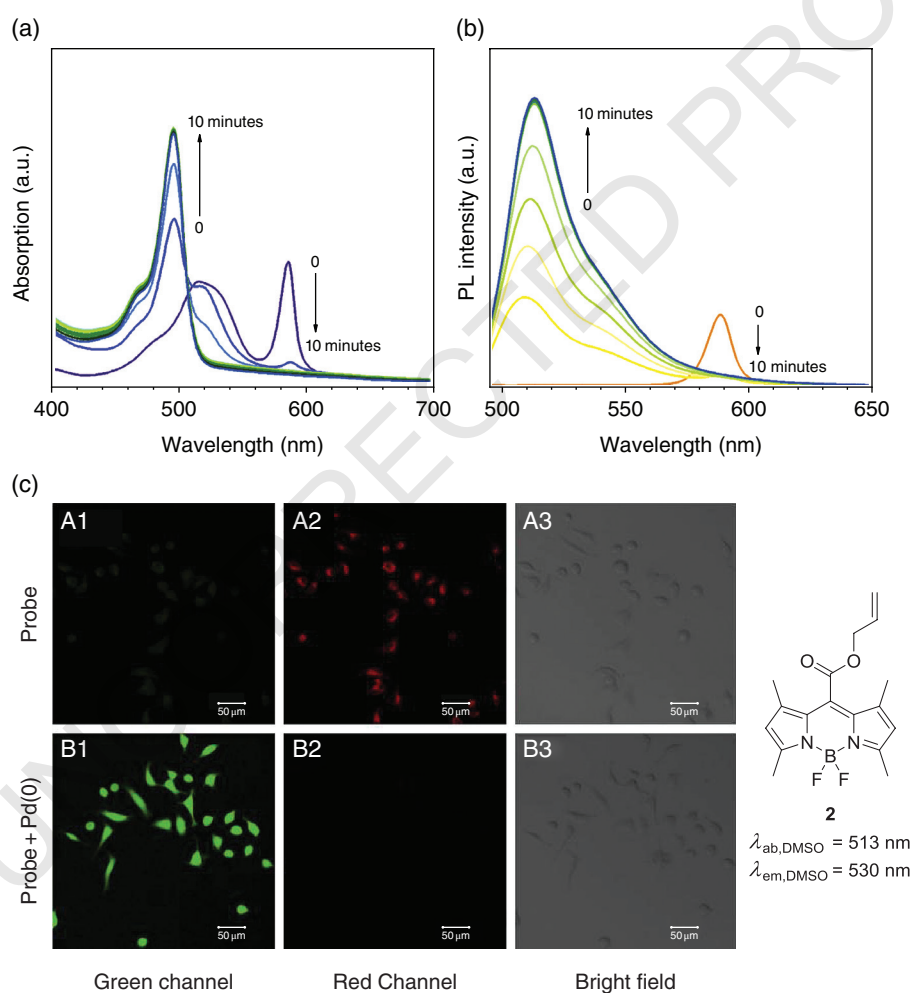


**Figure 18.35** (a) Absorption spectra recorded for 10  $\mu\text{M}$  solutions of **2** upon addition of  $\text{Pd}(\text{PPh}_3)_4$  in phosphate buffer solution at 25 °C. (b) Fluorescence emission spectra of **2** upon addition of  $\text{Pd}(\text{PPh}_3)_4$  in phosphate buffer solution. (c) Confocal fluorescence images of **2** to  $\text{Pd}(\text{PPh}_3)_4$  in HeLa cells. Source: Reproduced from Ref. [30]. Copyright 2019 Elsevier Ltd.

green with the emission peak located at 513 nm. Pd(0) may trigger the cleavage of *meso*-ester group to *meso*-carboxylate anion to cause the significant emission enhancement at 513 nm. Furthermore, compound **2** is also suitable for imaging of intracellular Pd(0) in a dual-channel responsive manner. When the dye is incubated with HeLa cells, intense red fluorescence is observed through the red channel, and almost no emission can be observed from the green channel. When Pd(0) is coin-cubated, bright-green emission is turned on in the green channel, accompanying with a decrease in fluorescence intensity in the red channel.

## 18.5 Conclusion

In this chapter, diverse AIE-active BODIPY derivatives – the widely explored organic luminescent materials with unique photophysical properties in the aggregated state are summarized. The popular approach to turn BODIPY compounds to AIE-active is to introduce AIEgens such as tetraphenylethene and triphenylamines to the BODIPY derivatives through conjugated or nonconjugated linkages. Besides the advantages of photophysical properties inherited from BODIPY structures such as high molar extinction coefficient, narrow emission peak, high photostability, these AIE-active BODIPYs also enjoy satisfied aggregated state emission. TICT processes are generally involved in these BODIPYs with electron donor/acceptor structures, resulting in red-shifted emission. It should be noted that the introduction of AIEgens into the BODIPY structure does not guarantee the AIE property of the resultant compounds. The systematic structure–property relationship study of the photophysical properties of these AIEgen-modified BODIPYs reveals that the emission behavior and aggregation-induced emission property of these BODIPYs are highly dependent on the substitution position and the linking spacers. Generally, AIEgen attached on the *meso*-position of the BODIPY core is effective to bring AIE property. With careful design of the molecular structures, these AIE-active BODIPYs can show fluorescence sensitivity toward a series of external stimuli including mechanical force, organic vapors, acid or base, viscosity and temperature, anions such as F<sup>−</sup> and CN<sup>−</sup>, H<sub>2</sub>S, biothiols, palladium species, and so on, which can find potential applications as smart materials and in vitro or in vivo bioprobes. Through combination of AIE property and the unique photophysical property of BODIPYs, the luminescent materials are expected to find large potential in diverse application fields.

## AQ8 References

- 1 N. Boens, V. Leen, W. Dehaen, *Chem. Soc. Rev.* 2012, 41, 1130–1172.
- 2 S. Kim, H. E. Pudavar, A. Bonoiu, P. N. Prasad, *Adv. Mater.* 2007, 19, 3791–3795.
- 3 G. Ulrich, R. Ziessel, A. Harriman, *Angew. Chem. Int. Ed.* 2008, 47, 1184–1201.
- 4 R. Ziessel, G. Ulrich, A. Harriman, *N. J. Chem.* 2007, 31, 496–501.
- 5 A. Loudet, K. Burgess, *Chem. Rev.* 2007, 107, 4891–4932.
- 6 A. Treibs, F. H. Kreuzer, *Justus Liebigs Ann. Chem.* 1968, 718, 208–223.
- 7 Q. Zheng, G. S. He, P. N. Prasad, *Chem. Phys. Lett.* 2009, 475, 250–255.
- 8 J. Bañuelos, F. L. Arbeloa, V. Martinez, M. Liras, A. Costela, I. G. Moreno, I. L. Arbeloa, *Phys. Chem. Chem. Phys.* 2011, 13, 3437–3445.
- 9 R. Ziessel, B. D. Allen, D. B. Rewinska, A. Harriman, *Chem. Eur. J.* 2009, 15, 7382–7393.
- 10 T. Bura, N. Leclerc, S. Fall, P. Lévêque, T. Heiser, P. Retailleau, S. Rihn, A. Mirloup, R. Ziessel, *J. Am. Chem. Soc.* 2012, 134, 17404–17407.

- 11 R. Ziessel, G. Ulrich, K. J. Elliott, A. Harriman, *Chem. Eur. J.* 2009, 15, 4980–4984.
- 12 R. Ziessel, A. Harriman, *Chem. Commun.* 2011, 47, 611–631.
- 13 L. Bonardi, H. Kanaan, F. Camerel, P. Jolinat, P. Retailleau, R. Ziessel, *Adv. Funct. Mater.* 2008, 18, 401–413.
- 14 Y. Ueno, J. Jose, A. Loudet, C. Pérez-Bolívar, P. Anzenbacher Jr, K. Burgess, *J. Am. Chem. Soc.* 2011, 133, 51–55.
- 15 Y. Qian, L. Zhang, S. Ding, X. Deng, C. He, X. E. Zheng, H.-L. Zhu, J. Zhao, *Chem. Sci.* 2012, 3, 2920–2923.
- 16 A. Coskun, E. U. Akkaya, *J. Am. Chem. Soc.* 2006, 128, 14474–14475.
- 17 R. Wang, F. Yu, P. Liu, L. Chen, *Chem. Commun.* 2012, 48, 5310–5312.
- 18 I. J. Arroyo, R. Hu, G. Merino, B. Z. Tang, E. Peña-Cabrera, *J. Org. Chem.* 2009, 74, 5719–5722.
- 19 Y. Gabe, Y. Urano, K. Kikuchi, H. Kojima, T. Nagano, *J. Am. Chem. Soc.* 2004, 126, 3357–3367.
- 20 Z. X. Zhang, X. F. Guo, H. Wang, H. S. Zhang, *Anal. Chem.* 2015, 87, 3989–3995.
- 21 J. Bartelmess, M. Baldrighi, V. Nardone, E. Parisini, D. Buck, L. Echegoyen, S. Giordani, *Chem. Eur. J.* 2015, 21, 9727–9732.
- 22 Y. Hong, J. W. Lam, B. Z. Tang, *Chem. Soc. Rev.* 2011, 40, 5361–5388.
- 23 Y. Hong, J. W. Lam, B. Z. Tang, *Chem. Commun.* 2009, 4332–4353.
- 24 J. Mei, N. L. Leung, R. T. Kwok, J. W. Lam, B. Z. Tang, *Chem. Rev.* 2015, 115, 11718–11940.
- 25 R. Hu, E. Lager, A. Aguilar-Aguilar, J. Liu, J. W. Y. Lam, H. H. Y. Sung, I. D. Williams, Y. Zhong, K. S. Wong, E. Peña-Cabrera, et al., *J. Phys. Chem. C* 2009, 113, 15845–15853.
- 26 E. Palao, S. de la Moya, A. R. Agarrabeitia, I. Esnal, J. Banelos, I. Lopez-Arbeloa, M. J. Ortiz, *Org. Lett.* 2014, 16, 4364–4367.
- 27 L. Jiao, C. Yu, J. Wang, E. A. Briggs, N. A. Besley, D. Robinson, M. J. Ruedas-Rama, A. Orte, L. Crovetto, E. M. Talavera, et al., *RSC Adv.* 2015, 5, 89375–89388.
- 28 I. J. Arroyo, R. Hu, B. Z. Tang, F. I. López, E. Peña-Cabrera, *Tetrahedron* 2011, 67, 7244–7250.
- 29 S. Choi, J. Bouffard, Y. Kim, *Chem. Sci.* 2014, 5, 751–755.
- 30 J. Zhou, S. Xu, Z. Yu, X. Ye, X. Dong, W. Zhao, *Dyes Pigm.* 2019, 170, 107656.
- 31 S. V. Mulay, T. Yudhistira, M. Choi, Y. Kim, J. Kim, Y. J. Jang, S. Jon, D. G. Churchill, *Chem. Asian J.* 2016, 11, 3598–3605.
- 32 C. Yu, Z. Huang, W. Gu, Q. Wu, E. Hao, Y. Xiao, L. Jiao, W.-Y. Wong, *Mater. Chem. Front.* 2019, 3, 1823–1832.
- 33 Y. Zhao, S. He, J. Yang, H. Sun, X. Shen, X. Han, Z. Ni, *Opt. Mater.* 2018, 81, 102–108.
- 34 M. Baglan, S. Ozturk, B. Gür, K. Meral, U. Bozkaya, O. A. Bozdemir, S. Atilgan, *RSC Adv.* 2013, 3, 15866–15874.
- 35 Z. Li, Y. Chen, X. Lv, W. F. Fu, *N. J. Chem.* 2013, 37, 3755–3761.
- 36 R. Wang, W. Gao, J. Gao, G. Xu, T. Zhu, X. Gu, C. Zhao, *Front. Chem.* 2019, 7, 778.
- 37 H. Ma, Z. Zhang, Y. Jin, L. Zha, C. Qi, H. Cao, Z. Yang, Z. Yang, Z. Lei, *RSC Adv.* 2015, 5, 87157–87167.
- 38 Q. Wang, X. Wei, C. Li, Y. Xie, *Dyes Pigm.* 2018, 148, 212–218.
- 39 X. Xu, Y. Qian, *J. Lumin.* 2018, 202, 206–211.
- 40 Q. Li, Y. Qian, *J. Photochem. Photobiol. Chem.* 2017, 336, 183–190.
- 41 L. Wang, L. Li, D. Cao, *Sens. Actuators B Chem.* 2017, 241, 1224–1234.
- 42 W. Che, G. Li, J. Zhang, Y. Geng, Z. Xie, D. Zhu, Z. Su, *J. Photochem. Photobiol. Chem.* 2018, 358, 274–283.
- 43 S. Sengupta, U. K. Pandey, *Org. Biomol. Chem.* 2018, 16, 2033–2038.
- 44 S. Sengupta, U. K. Pandey, E. U. Athresh, *RSC Adv.* 2016, 6, 73645–73649.
- 45 P. Aswathy, S. Sharma, N. P. Tripathi, S. Sengupta, *Chem. Eur. J.* 2019, 25, 14870–14880.

- 46 R. Singh, K. N. Unni, A. Solanki, others, *Opt. Mater.* 2012, 34, 716–723.
- 47 G. W. Zhang, P. F. Li, Z. Meng, H. X. Wang, Y. Han, C. F. Chen, *Angew. Chem. Int. Ed.* 2016, 55, 5304–5308.
- 48 S. Zhang, Y. Wang, F. Meng, C. Dai, Y. Cheng, C. Zhu, *Chem. Commun.* 2015, 51, 9014–9017.
- 49 J. Roose, B. Z. Tang, K. S. Wong, *Small.* 2016, 12, 6495–6512.
- 50 H. T. Feng, X. Gu, J. W. Lam, Y. S. Zheng, B. Z. Tang, *J. Mater. Chem. C* 2018, 6, 8934–8940.
- 51 T. R. Cook, V. Vajpayee, M. H. Lee, P. J. Stang, K. W. Chi, *Acc. Chem. Res.* 2013, 46, 2464–2474.
- 52 R. Liu, S. Zhu, J. Lu, H. Shi, H. Zhu, *Dyes Pigm.* 2017, 147, 291–299.
- 53 G. Gupta, A. Das, N. B. Ghate, T. Kim, J. Y. Ryu, J. Lee, N. Mandal, C. Y. Lee, *Chem. Commun.* 2016, 52, 4274–4277.
- 54 K. Shimizu, D. Kitagawa, S. Kobatake, *Dyes Pigm.* 2019, 161, 341–346.
- 55 D. Yang, S. Zhang, Y. Hu, J. Chen, B. Bao, L. Yuwen, L. Weng, Y. Cheng, L. Wang, *RSC Adv.* 2016, 6, 114580–114586.
- 56 Z. Wang, Y. Feng, N. Wang, Y. Cheng, Y. Quan, H. Ju, *J. Phys. Chem. Lett.* 2018, 9, 5296–5302.
- 57 H. Yamane, S. Ito, K. Tanaka, Y. Chujo, *Polym. Chem.* 2016, 7, 2799–2807.
- 58 B. K. Dwivedi, R. S. Singh, A. Ali, V. Sharma, S. M. Mobin, D. S. Pandey, *Analyst* 2019, 144, 331–341.
- 59 Z. Zhang, B. Xu, J. Su, L. Shen, Y. Xie, H. Tian, *Angew. Chem. Int. Ed.* 2011, 50, 11654–11657.
- 60 Y. Zhang, X. Zheng, L. Zhang, Z. Yang, L. Chen, L. Wang, S. Liu, Z. Xie, *Org. Biomol. Chem.* 2020, 18, 707–714.
- 61 J. Qiu, S. Jiang, H. Guo, F. Yang, *Dyes Pigm.* 2018, 157, 351–358.
- 62 R. S. Singh, A. Kumar, S. Mukhopadhyay, G. Sharma, B. Koch, D. S. Pandey, *J. Phys. Chem. C* 2016, 120, 22605–22614.
- 63 Y. Bai, D. Liu, Z. Han, Y. Chen, Z. Chen, Y. Jiao, W. He, Z. Guo, *Sci. China Chem.* 2018, 61, 1413–1422.
- 64 X. Zhu, R. Liu, Y. Li, H. Huang, Q. Wang, D. Wang, X. Zhu, S. Liu, H. Zhu, *Chem. Commun.* 2014, 50, 12951–12954.
- 65 L. Li, L. Wang, H. Tang, D. Cao, *Chem. Commun.* 2017, 53, 8352–8355.
- 66 Q. Liu, X. Wang, H. Yan, Y. Wu, Z. Li, S. Gong, P. Liu, Z. Liu, *J. Mater. Chem. C.* 2015, 3, 2953–2959.
- 67 X. Wang, Y. Wu, Q. Liu, Z. Li, H. Yan, C. Ji, J. Duan, Z. Liu, *Chem. Commun.* 2015, 51, 784–787.
- 68 W. Duan, Q. Liu, Y. Huo, J. Cui, S. Gong, Z. Liu, *Org. Biomol. Chem.* 2018, 16, 4977–4984.
- 69 C. W. Liao, R. Rao M., S. S. Sun, *Chem. Commun.* 2015, 51, 2656–2659.
- 70 R. Hu, C. F. A. Gómez-Durán, J. W. Y. Lam, J. L. Belmonte-Vázquez, C. Deng, S. Chen, R. Ye, E. Peña-Cabrera, Y. Zhong, K. S. Wong, et al., *Chem. Commun.* 2012, 48, 10099.
- 71 C. F. A. Gomez-Duran, R. Hu, G. Feng, T. Li, F. Bu, M. Arseneault, B. Liu, E. Peña-Cabrera, B. Z. Tang, *ACS Appl. Mater. Interf.* 2015, 7, 15168–15176.
- 72 Z. Zhao, B. Chen, J. Geng, Z. Chang, L. Aparicio-Ixta, H. Nie, C. C. Goh, L. G. Ng, A. Qin, G. Ramos-Ortiz, et al., *Part. Part. Syst. Charact.* 2014, 31, 481–491.
- 73 M. H. Chua, Y. Ni, M. Garai, B. Zheng, K. W. Huang, Q. H. Xu, J. Xu, J. Wu, *Chem. Asian J.* 2015, 10, 1631–1634.
- 74 C. Yang, J. H. Lee, C. Chen, *J. Chin. Chem. Soc.* 2019, 66, 1199–1210.
- 75 W. Che, L. Zhang, Y. Li, D. Zhu, Z. Xie, G. Li, P. Zhang, Z. Su, C. Dou, B. Z. Tang, *Anal. Chem.* 2019, 91, 3467–3474.
- 76 L. Zhang, Y. Chen, J. Jiang, *Dyes Pigm.* 2016, 124, 110–119.
- 77 S. Baysec, A. Minotto, P. Klein, S. Poddi, A. Zampetti, S. Allard, F. Cacialli, U. Scherf, *Sci. China Chem.* 2018, 61, 932–939.
- 78 J. Wu, W. Liu, J. Ge, H. Zhang, P. Wang, *Chem. Soc. Rev.* 2011, 40, 3483–3495.

- 79 D. Su, J. Oh, S. C. Lee, J. M. Lim, S. Sahu, X. Yu, D. Kim, Y. T. Chang, *Chem. Sci.* 2014, 5, 4812–4818.
- 80 D. Su, C. L. Teoh, N. Y. Kang, X. Yu, S. Sahu, Y. T. Chang, *Chem. Asian J.* 2015, 10, 581–585.
- 81 E. Şen, K. Meral, S. Atılğan, *Chem. Eur. J.* 2016, 22, 736–745.
- 82 L. Lin, X. Lin, H. Guo, F. Yang, *Org. Biomol. Chem.* 2017, 15, 6006–6013.
- 83 R. S. Singh, R. K. Gupta, R. P. Paitandi, M. Dubey, G. Sharma, B. Koch, D. S. Pandey, *Chem. Commun.* 2015, 51, 9125–9128.
- 84 B. Dhokale, T. Jadhav, S. M. Mobin, R. Misra, *J. Org. Chem.* 2015, 80, 8018–8025.
- 85 R. Vedarajan, Y. Hosono, N. Matsumi, *Solid State Ion.* 2014, 262, 795–800.



UNCORRECTED PROOFS